

[Click here to view linked References](#)

1           **Stochastic source, path and site attenuation parameters and**  
2           **associated variabilities for shallow crustal European earthquakes**

3    By

4    Sanjay Singh Bora<sup>1\*</sup>, Fabrice Cotton<sup>1,2</sup>, and Frank Scherbaum<sup>1,2</sup>, Benjamin Edwards<sup>3</sup>,  
5    Paola Traversa<sup>4</sup>

6    \*Corresponding author:

7    Email: [bora@gfz-potsdam.de](mailto:bora@gfz-potsdam.de)

8    <sup>1</sup> GFZ German Research Center for Geosciences, Potsdam, Germany

9    <sup>2</sup> University of Potsdam, Potsdam, Germany

10   <sup>3</sup> Department Earth, Ocean and Ecological Sciences, University of Liverpool, UK

11   <sup>4</sup> French Electric Company, Aix-en-Provence France

12   Submission to Bulletin of Earthquake Engineering

13   Potsdam, September 9, 2016

14

15 **Abstract** We have analyzed the recently developed pan-European strong motion  
16 database, RESORCE-2012: spectral parameters, such as stress drop (stress parameter,  
17  $\Delta\sigma$ ), anelastic attenuation ( $Q$ ), near surface attenuation ( $\kappa_0$ ) and site amplification have  
18 been estimated from observed strong motion recordings. The selected dataset exhibits a  
19 bilinear distance-dependent  $Q$  model with average  $\kappa_0$  value 0.0308 s. Strong regional  
20 variations in inelastic attenuation were also observed: frequency-independent  $Q_0$  of  
21 1462 and 601 were estimated for Turkish and Italian data respectively. Due to the  
22 strong coupling between  $Q$  and  $\kappa_0$ , the regional variations in  $Q$  have strong impact on  
23 the estimation of near surface attenuation  $\kappa_0$ .  $\kappa_0$  was estimated as 0.0457 and 0.0261s  
24 for Turkey and Italy respectively. Furthermore, a detailed analysis of the variability in  
25 estimated  $\kappa_0$  revealed significant within-station variability. The linear site  
26 amplification factors were constrained from residual analysis at each station and site-  
27 class type. Using the regional  $Q_0$  model and a site-class specific  $\kappa_0$ , seismic moments  
28 ( $M_0$ ) and source corner frequencies  $f_c$  were estimated from the site corrected empirical  
29 Fourier spectra.  $\Delta\sigma$  did not exhibit magnitude dependence. The median  $\Delta\sigma$  value was  
30 obtained as 5.75 and 5.65 MPa from inverted and database magnitudes respectively. A  
31 comparison of response spectra from the stochastic model (derived herein) with that  
32 from (regional) ground motion prediction equations (GMPEs) suggests that the  
33 presented seismological parameters can be used to represent the corresponding  
34 seismological attributes of the regional GMPEs in a host-to-target adjustment  
35 framework. The analysis presented herein can be considered as an update of that  
36 undertaken for the previous Euro-Mediterranean strong motion database presented by  
37 Edwards and Fäh (2013a).

38 **Keywords:** Stochastic model, attenuation, stress parameter, kappa, crustal earthquakes

## 39 **1. Introduction**

40 Estimation of regional seismological attributes such as source, path and site specific  
41 parameters is important in a wide range of applications in seismic hazard analysis.  
42 Usually, in engineering seismology and seismic hazard studies strong ground motions  
43 (specifically accelerations) are modeled in terms of a stochastic process (Hanks 1979;  
44 McGuire and Hanks 1980; Hanks and McGuire 1981) assuming that phases of high  
45 frequency waves (ground motions) are random. Typically, the stochastic (amplitude)  
46 model is characterized in terms of magnitude and stress parameter ( $\Delta\sigma$ ) as being the  
47 source parameters; the geometrical spreading and anelastic attenuation ( $Q$ ) of seismic

48 wave describe the path effects. The site effects are modeled in terms of crustal  
49 amplification (Boore 2003; Joyner et al. 1981; Boore and Joyner 1997) and site-related  
50 attenuation parameter ( $\kappa_0$ ).

51 We have analyzed the recently developed pan-European strong motion database,  
52 RESORCE-2012 (Akkar et al. 2014a) in order to estimate these spectral parameters. In  
53 addition to estimate these seismological parameters that describe the amplitude and  
54 shape of Fourier spectra of strong ground motion, we also focus our discussion on  
55 variability and trade-off issues. More specifically, we analyze the following key issues  
56 related with the stochastic modelling of ground motion:

57 (1) A European stochastic model has been derived by Edward and Fäh (2013a). This  
58 model was based upon a strong-motion database compiled more than a decade ago  
59 and, due to limited data, did not include regional variations in attenuation  
60 properties within Europe. The analysis of more recent strong-motion database  
61 indicates that regional variations of ground motions may be significant (Boore et  
62 al. 2014; Kotha et al. 2016; Kuehn and Scherbaum 2016) which is a motivation to  
63 evaluate the regional variations of stochastic ground motions parameters in Europe.

64 (2) One of the major challenges in ground motion prediction is that motions need to be  
65 predicted for earthquakes without knowing the (future) stress-parameter ( $\Delta\sigma$ )  
66 associated with them. Therefore, usually blind predictions are made for an average  
67 value of  $\Delta\sigma$  with an associated standard deviation. Often, the average  $\Delta\sigma$  is  
68 assumed to be independent of magnitude (Aki 1967), however recent studies have  
69 indicated, that for small to moderate earthquakes ( $M_W < 5$ )  $\Delta\sigma$  may increase with  
70 increasing magnitude and the average  $\Delta\sigma$  can also vary regionally (Malagnini et al.  
71 2008; Edwards et al. 2008; Drouet et al. 2008; Drouet et al. 2010; Yenier and  
72 Atkinson 2015a; Yenier and Atkinson 2015b). Other than the magnitude  
73 dependence and regional variation, the spread (standard deviation) in estimated  $\Delta\sigma$   
74 is also important in predicting ground motions for future scenarios (Cotton et al.  
75 2013).

76 (3) The decay of high frequency Fourier spectral amplitudes beyond the Brune's  
77 corner frequency  $f_c$  is usually attributed to (an empirical parameter)  $\kappa$  (kappa)  
78 (Anderson and Hough 1984) that essentially captures the combined effect of whole  
79 path anelastic attenuation ( $Q$ ) and near site attenuation  $\kappa_0$ . Extrapolation of  $\kappa$  at  
80 near distances ( $\approx$  zero) is termed as  $\kappa_0$  and is believed to reflect near site

81 attenuation. In a site-specific seismic hazard application, knowing  $\kappa_0$  beforehand at  
82 a target site is of crucial importance. As shown by Molkenhain et al. (2014) and  
83 Douglas and Jousset (2011) in a stochastic simulation framework, pseudo spectral  
84 accelerations (PSA) for small to moderate events at high oscillator frequencies  $>10$   
85 Hz are mainly controlled by  $\kappa_0$ . However, measurement of a true site  $\kappa_0$  is not  
86 straightforward because the observed traces are recorded at a non-zero distance,  
87 which makes decoupling of path term ( $Q$ ) and  $\kappa_0$  rather challenging without  
88 constraining any of the two *a priori*. In this context, regional variation of  $Q$ , as will  
89 be shown in this article, can also bias the estimation of  $\kappa_0$ . Thus, the trade-off  
90 between  $Q$  and  $\kappa_0$  needs to be analyzed and accounted in the forward prediction as  
91 well.

92 (4) Several studies have shown that  $\kappa_0$  varies significantly from site-to-site and  
93 regionally as well (e.g., Atkinson and Morrison 2009; Edwards et al. 2008;  
94 Campbell 2009; Edwards and Rietbrock 2009). The site-to-site/station-to-station  
95 variability of  $\kappa_0$  will be referred as between-station variability. The other  
96 component of variability in  $\kappa_0$  is related to the record-to-record (or within-station)  
97 variability. Within-station variability of  $\kappa_0$  can also have a strong impact on the  
98 site-to-site adjustment of GMPEs in the HTTA framework. However, this within-  
99 station variability has not been discussed much in past studies.

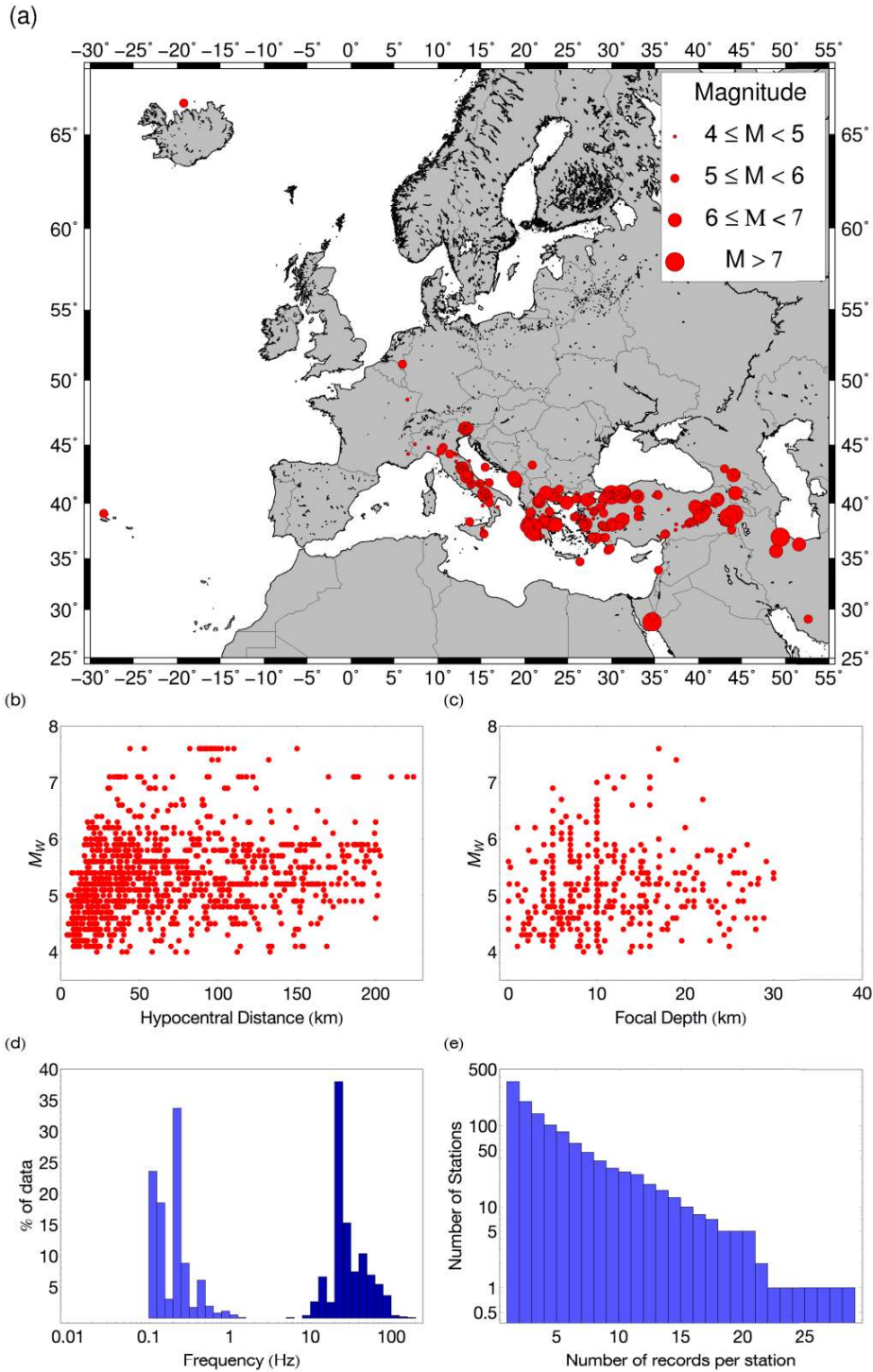
100 Assuming  $\omega^2$  point-source model (Brune 1970, 1971) – which has been shown to be  
101 applicable to  $M_W < 6$  events globally, and a reasonable approximation for larger  
102 events at high frequencies (Chen and Atkinson 2002; Baltay and Hanks 2014) – a  
103 broadband (generalized) inversion technique (Edwards and Fäh 2013a; Bora et al.  
104 2015) is performed to determine the source, path and site parameters.

105 Essentially, the inversion method remains the same as detailed in Bora et al. (2015) in  
106 which a full Fourier amplitude spectrum is used to estimate Brune's source corner  
107 frequency ( $f_c$ ) and the whole path inelastic attenuation operator ( $t^*$ ) simultaneously.  
108 The inverted  $t^*$  values are further analyzed to derive a frequency-independent  $Q_0$   
109 model for the dataset and to analyze regional variation in  $Q_0$  within the selected  
110 dataset. The choice of a particular  $Q_0$  model is seen to have a large impact on the  
111 derived  $\kappa_0$  values. With respect to the regional  $Q_0$  models, we investigated two  
112 different components of variability in station  $\kappa_0$  in terms of station-to station  
113 variability (between-station) and record-to-record variability (within-station). After

114 constraining the reference model by using the database  $M_0$  and regional inelastic  
115 attenuation  $Q_0$  models, average residuals are used to capture the linear part of the site  
116 amplification in the Fourier domain (Edwards et al. 2013; Drouet et al. 2010; Poggi et  
117 al. 2011). The final estimation of source  $f_c$  and  $M_0$  is obtained from site-effects  
118 corrected spectra, which are further analyzed to estimate stress parameter ( $\Delta\sigma$ ) values.

## 119 **2. Data**

120 Different subsets of the RESORCE-2012 database have been used to derive several  
121 pan-European GMPEs (Akkar et al. 2014b; Bindi et al. 2014; Bora et al. 2014; Derras  
122 et al. 2014; and Hermkes et al. 2014). The same dataset as used by Bora et al. (2015) is  
123 used in this study. This dataset is a subset of a larger parent database of RESORCE-  
124 2012 (Akkar et al. 2014a) and it contains strong motion recordings made across  
125 Europe, the Mediterranean region and the Middle East. To ensure the validity of the  
126 point-source (Brune model) approximation, we have discarded near distance traces  
127 from large magnitude earthquakes (Bora et al. 2015). For events with moment  
128 magnitude  $M_W < 5.5$  no trace was discarded; for events with  $5.5 \leq M_W < 6.5$  traces  
129 recorded at hypocentral distance  $R < 15$  km were discarded; and for  $M_W \geq 6.5$ , traces  
130 recorded at  $R < 30$  km were not considered. The dataset consists of 1200 (2400  
131 including both the horizontal components) acceleration traces recorded at 350 stations  
132 from 365 earthquakes. Figure 1 summarizes the main metadata features of the selected  
133 dataset. Figure 1a depicts geographical distribution of epicenters from the selected  
134 dataset. The magnitude and distance range covered by the present dataset is  $M_W$  4-7.6  
135 and hypocentral distance up to 224 km respectively (Figure 1b). The station  $Vs_{30}$   
136 values range from 92 to 2165 m/s out of which 223 are measured and rest are inferred  
137 from different methods. All the events are shallow crustal events up to the focal depth  
138 of 30 km (Figure 1c). For complete metadata information of the recordings, the reader  
139 is referred to the electronic supplement supplied with Bora et al. (2015). The processed  
140 database was disseminated to ensure a uniform data processing scheme for empirical  
141 ground motion prediction equation (GMPE) derivation.



142

143 **Figure 1.** Metadata summary of the selected dataset. (a) Distribution of earthquake epicenters; (b)  $M_W$ -hypocentral  
 144 distance distribution; (c)  $M_W$ -depth distribution; (d) light-shade: high-pass and dark-shade: low-pass frequency;  
 145 (e) number of records per station versus number of stations.

146

147

148

Additionally, for our analysis we use the Fourier amplitudes only between the useable  
 frequency limits. We chose the filter high-pass and low-pass frequencies as the useable  
 frequency limits, if a record is not assigned a low-pass frequency in the metadata then

149 a flat low-pass frequency of 50 Hz was chosen. It is worth mentioning here that no  
 150 smoothing is applied over the observed Fourier spectral amplitudes prior to the  
 151 inversion except that the amplification curves are presented after smoothing (Konno  
 152 and Ohmachi 1998) observed Fourier amplitude spectra. Figure 1d shows the  
 153 distribution of high-pass and low-pass frequencies in the dataset, while Figure 1e  
 154 depicts the number of records per station against the number of stations.

### 155 **3. Fourier Spectral Inversion**

156 We use the Brune's (1970, 1971) point source model with a single corner frequency  
 157 ( $f_c$ ) to characterize the far field Fourier spectrum of acceleration records. In the  
 158 stochastic modelling framework (Boore 1983, 2003), assuming that the high frequency  
 159 ground motions of engineering interests are randomly distribution in phase the Fourier  
 160 spectral amplitude  $Y$  at a frequency,  $f$  can be modeled using the following analytical  
 161 relationship (Bora et al. 2015):

$$162 \quad Y(f) = CM_0G(R) \left\{ \frac{(2\pi f)^2}{1 + \left(\frac{f}{f_c}\right)^2} \right\} e^{-\pi f t^*} A(f). \quad (1)$$

163 In equation (1),  $M_0$  is the seismic moment in units of  $Nm$  and  $f_c$  is the corner  
 164 frequency in Hertz, given by  $0.4906\beta(\Delta\sigma/M_0)^{1/3}$  (Eshelby 1957; Brune 1970, 1971),  
 165 in which  $\Delta\sigma$  is the stress parameter in Mega Pascal and  $\beta$  ( $= 3500$  m/s) is the shear  
 166 wave velocity in the vicinity of the source. The constant  $C$  is generally taken as  
 167  $\Theta_{\lambda\phi}F\xi/(4\pi\rho\beta^3)$ , in which  $\Theta_{\lambda\phi}$  ( $= 0.55$ ) is the average radiation pattern for S waves  
 168 (Boore and Boatwright 1984),  $F$  ( $= 2.0$ ) is the near surface amplification,  $\xi$  ( $= 1/\sqrt{2}$ ) is  
 169 a factor to account for the partition of total shear-wave energy into two horizontal  
 170 components, and  $\rho$  ( $= 2800$  kg/m<sup>3</sup>) is the average density near the source (Boore 1983,  
 171 2003).  $G(R)$  is the geometrical spreading function representing a frequency-  
 172 independent decay of amplitude as function of distance. Theoretically,  $G(R)$  is equal to  
 173  $1/R$  at near distances ( $< \sim 50$ - $100$  km) for an isotropic and homogenous whole space.  
 174 However, the earth is not homogeneous and many studies have found it to be a  
 175 complex function of distance (Campillo et al. 1984; Atkinson and Mereu 1992;  
 176 Edwards et al. 2008; Atkinson and Boore 2011). To limit potential trade-off and bias,  
 177  $G(R)$  is constrained by using an earlier derived  $G(R)$  model from the same dataset in  
 178 Bora et al. (2015) as:

$$179 \quad G(R) = \begin{cases} \left(\frac{R_0}{R}\right)^{1.14} & R \leq 70 \\ \left(\frac{R_0}{R_1}\right)^{1.14} \left(\frac{R_1}{R}\right)^{0.5} & R > 70 \end{cases} \quad (2)$$

180 In equation (2),  $R_0$  is assumed to be 1 km. Bora et al. (2015) derived the  $G(R)$  model  
 181 from low-frequency (0.2-1 Hz) Fourier spectral amplitudes to minimize the trade-off  
 182 resulting from high-frequency attenuation  $Q$ .

183 The fall-off of acceleration spectra at high frequencies is modeled by using a whole-  
 184 path anelastic attenuation operator ( $t^*$ ).  $t^*$  is alternatively named  $\kappa(R)$  (Anderson and  
 185 Hough, 1984) and  $\kappa_r$  (Ktenidou et al. 2014). The  $t^*$  implies spectral decay at high  
 186 frequencies due to path and site effects, while some authors (e.g., Kilb et al. 2012)  
 187 argue contribution of source effects in  $t^*$  as well. The combined effect of anelastic  
 188 attenuation  $Q$  and site-related attenuation  $\kappa_0$  (Ktenidou et al. 2014) in  $t^*$  is represented  
 189 by the following equation:

$$190 \quad t^* = \frac{R}{Q\beta} + \kappa_0 \quad (3)$$

191 in which  $\beta$  (= 3.5 km/s) is the average shear wave velocity used to infer  $Q$  and  $R$  is the  
 192 hypocentral distance. Some studies have suggested (Singh et al. 1982; Atkinson and  
 193 Mereu 1992; Malagnini et al. 2000; Bay et al. 2003; Atkinson 2004; Drouet et al. 2008;  
 194 Malagnini et al. 2011; Akinici et al. 2014) a  $Q$  model as a function of frequency as  
 195 follows:

$$196 \quad Q(f) = Q_0 \left(\frac{f}{f_0}\right)^\eta \quad (4)$$

197 in which,  $\eta$  ranges from 0, for a frequency-independent  $Q$ , to 1 and  $Q_0$  is the reference  
 198  $Q$  value at  $f_0 = 1$  Hz. However, estimation of  $Q$  from spectra of observed recordings is  
 199 strongly tied with the assumed geometrical spreading (e.g. Pacor et al. 2016). As  
 200 shown by Edwards et al. (2008, 2011) a frequency-dependent  $Q$  function can lead to a  
 201 strong trade-off with the geometrical spreading. Furthermore, Morozov (2008, 2009)  
 202 have suggested that from a modeling perspective distinction between frequency-  
 203 dependent  $Q$  and geometric attenuation is ambiguous. Thus, some studies (Anderson  
 204 and Hough 1984; Hough et al. 1988; Edwards et al. 2008, 2011; Campbell 2009;  
 205 Edwards and Fäh 2013a) in engineering seismology also use a frequency-independent  
 206  $Q = Q_0$  (constant) over the frequency-band it is measured. Thus in this article, we  
 207 restrict our model formulation to a constant- $Q$  model. It is beyond the scope of this



208 article to investigate sensitivity of a chosen  $Q$  model (frequency-independent or  
209 constant) over the parameters derived here, however a constant- $Q$  is expected to give  
210 lower  $\kappa_0$  value than that with a frequency-dependent  $Q$ . Nevertheless, the derived  
211 parameter values (with a constant- $Q$  assumption) are consistent within the entire model  
212 framework (taking geometrical spreading,  $\Delta\sigma$ ,  $Q_0$  and  $\kappa_0$  together).  $A(f)$  in equation  
213 (1) represents site amplification, which essentially captures the effect of impedance  
214 contrast during the wave propagation from the half-space through the upper soil layers  
215 to the station.

216 In our inversion scheme the observed spectra are inverted with respect to the natural  
217 log of the model described in equation (1) to determine  $M_0$ ,  $f_c$  and  $t^*$  using a least  
218 squares fit in which the Newton's method is used to linearize the nonlinear equation.  
219 To address the problem of two unresolved degrees of freedom, that is,  $M_0$  and  $A(f)$ , in  
220 the first iteration of inversion the low-frequency spectral level is constrained by using  
221  $M_0$  obtained from the database  $M_W$  (Hanks and Kanamori, 1979). Thus, database  $M_0$   
222 values and  $f_c$  and  $t^*$  determined from the first iteration of inversion, essentially  
223 describe our reference model. This reference model along with a generic crustal  
224 amplification function defines the motion at the base of the soil column beneath the  
225 station. The (logarithmic) difference between the observed amplitude and the  
226 amplitude obtained by the combination (addition in log) of reference model and the  
227 generic crustal amplification is used to constrain the amplification  $A(f)$  at a given  
228 station (for details see section Site Amplification). The final estimates of  $f_c$  and  $M_0$  are  
229 obtained from site-corrected,  $A(f)$ , spectra.

230 The inversion was performed over the full spectrum between the high-pass and low-  
231 pass frequencies of each record given in the metadata file. If a record is not assigned  
232 with a low-pass frequency then a flat low-pass frequency limit of 50 Hz is used. It is  
233 also known that site-effects can potentially bias the determination of seismological  
234 parameters from the surface recorded spectra. From records recorded at rock and hard  
235 rock site stations, determination of  $t^*$  can be biased due to significant resonance effects  
236 at high frequencies (Parolai and Bindi 2004; Edwards et al. 2015). Similarly, at soft  
237 soil sites, resonance effects present at low frequencies can bias the determination of  $f_c$ .  
238 However, in the present dataset majority of the earthquakes are of small to moderate  
239 magnitudes ( $M_W$  4–5.5), hence we believe that the corresponding  $f_c$  values will remain  
240 unaffected from the resonance effects. Furthermore, an event-wise (common for all

241 records originated from an event) determination of  $f_c$  can limit the potential bias due to  
242 the site-effects (Edwards et al. 2008). In order to limit bias in the determination of  $t^*$   
243 due to crustal amplification, we correct all the spectra for a reference rock  
244 amplification function (Bora et al. 2015; Edwards et al. 2015). Also, fitting the entire  
245 shape (determined by  $f_c$  and  $t^*$ ) of the spectrum simultaneously limits the error in  $t^*$   
246 estimation that may arise due to the resonance peaks at high frequencies. The majority  
247 of the stations in the selected dataset are located over soil or stiff-soil sites ( $180 <$   
248  $V_{S30} \leq 750$  m/s). The generic rock amplification of California (Boore and Joyner 1997)  
249 anchored at  $V_{S30}$  620 m/s was considered to be appropriate as reference rock  
250 amplification for the present dataset.

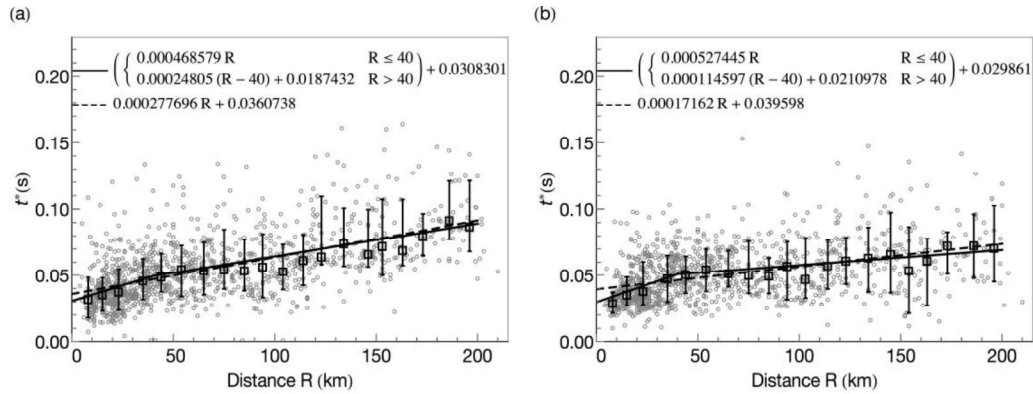
#### 251 **4. Attenuation Parameters: $t^*$ , $Q_0$ and $\kappa_0$**

252 As mentioned in the previous section, in the first step of our broadband inversion  
253 scheme we determine  $f_c$  and  $t^*$  simultaneously based upon the model described in  
254 equation (1) while seismic moments are constrained from database  $M_W$  values (Akkar  
255 et al. 2014a) using the relationship of Hanks and Kanamori (1979). In our analysis, we  
256 use hypocentral distance as the preferred distance metric, following Edwards and F ah  
257 (2013a). We obtain two  $t^*$  values per record, one for each component, however in  
258 order to limit the scatter in data points, a mean  $t^*$  (from both the components) is used  
259 here. Performing a least-squares linear fit using equation (3), over the dataset that  
260 contains  $t^*$  values against  $R$  (hypocentral distance), we find dataset common  $Q_0$   
261 (dividing the slope by  $\beta$ ) and  $\kappa_0$  (the intercept) values as 1029 and 0.0361s  
262 respectively. The 68% confidence interval of the best-fit slope corresponds to  $Q_0$   
263 values 982 and 1080. Similarly, the 68% confidence interval of the intercept gives  $\kappa_0$   
264 values of 0.035 and 0.0372s.

265 In terms of comparison between  $Q_0$  values from this study and those from earlier  
266 studies, Edwards and F ah (2013a) obtained the  $Q_0$  value as 619 from broadband fit  
267 using a smaller subset of the present dataset. In their study, Edwards and F ah (2013a)  
268 used records only up to 100 km of hypocentral distance. Edwards et al. (2011) and  
269 Douglas et al. (2010) presented  $Q_0$  values 1216 and 1630 for Switzerland and France  
270 respectively using the records up to 300 km; while in this study we use records up to  
271 224 km. Thus, this difference in  $Q_0$  values can be due to the differences arising from  
272 data-selection criteria, distance metric used and the actual regional difference in  $Q_0$ .

273 The choice of distance range in fitting  $t^*$ - $R$  data can also influence the estimated  $Q_0$   
274 values.

275 In order to further explore the distance dependent estimation of  $Q_0$ , we plot median of  
276 sorted (by distance)  $t^*$ - $R$  data in each 10 km distance bin, and as can be observed from  
277 Figure 2a a clear trend indicating distance-dependent attenuation,  $Q_0$ , (varying slope of  
278  $t^*$ - $R$  relationship) is visible. As a cross-check, we also analyzed the  $t^*$  values obtained  
279 from high-frequency linear fit method (Anderson and Hough 1984). The lower limit of  
280 the high-frequency range was selected (automatically) such that it is sufficiently above  
281 than the source  $f_c$  for each record for an assumed  $\Delta\sigma$  of 10 MPa and database  $M_W$ . The  
282 upper limit of the frequency range was either fixed to the low-pass frequency given in  
283 the metadata information or to 50 Hz for the records that are not assigned a low-pass  
284 frequency. Finally, only those  $t^*$  values were selected which were measured over a  
285 band of at least 10 Hz. The high frequency fit  $t^*$  values are plotted against distance in  
286 Figure 2b and a binning scheme similar to the one in Figure 2a was applied on the  $t^*$ - $R$   
287 data. A similar trend to that in Figure 2a can also be observed in Figure 2b indicating  
288 that the  $t^*$ - $R$  relationship from the selected dataset shows a distance-dependent slope  
289 (hence  $Q_0$ ). This observation was validated further from least square fit on the actual  
290  $t^*$ - $R$  data (without binning and averaging them) assuming a bilinear relationship with a  
291 slope-transition distance of 40 km. It can also be observed from Figures 2a and 2b that,  
292 the straight-line fit of  $t^*$ - $R$  data gives different zero-distance intercept,  $\kappa_0$ , whereas the  
293 values are rather identical for a bilinear fit. Hence a single linear fit model of  $t^*$ - $R$   
294 relationship might overestimate the  $\kappa_0$  values. Anderson (1991) has also suggested that  
295 if a straight line fit does not fit the data well, any other smooth functional form can be  
296 chosen. Selection of a bilinear form for  $t^*$ - $R$  relationship against more complicated  
297 (e.g., quadratic  $R$ ) forms was based upon a compromise between simplicity and  
298 effectiveness of the model in capturing the observed trend. Assuming an average  $\beta =$   
299 3.5 km/s, the  $Q_0$  values at  $R \leq 40$  and  $R > 40$  km were obtained as: 610 and 1152  
300 from broadband fit  $t^*$  and 542 and 2493 from high-frequency fit  $t^*$  values.



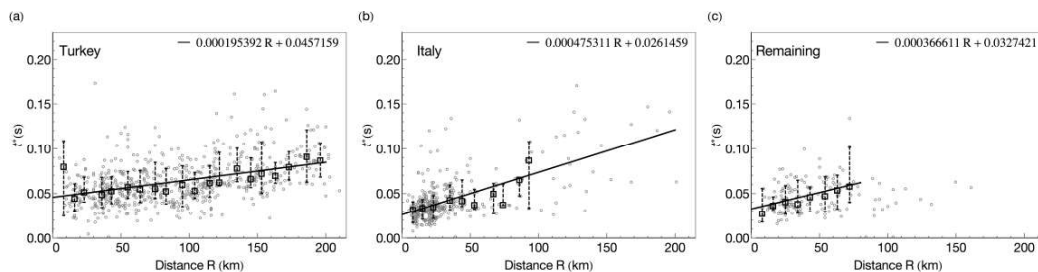
301

302 **Figure 2.**  $t^*$ -distance relationship from the entire dataset. (a) from broadband inversion method; (b) from high-  
 303 frequency linear fit method (Anderson and Hough 1984). The empty circles indicate the individual data points while  
 304 the empty squares indicate the median of  $t^*$ -R data in each 10 km distance bin. The extent of vertical bars indicate  
 305 the  $t^*$  values corresponding to 16 and 84 percentiles in each distance bin.

306 In order to investigate the regional variations in inelastic attenuation we split the  $t^*$ -R  
 307 data in three regional categories based upon the station locations: 1) stations located in  
 308 Turkey, 2) stations located in Italy and 3) the remaining stations in the dataset.  
 309 Although the physical properties are not expected to follow the political boundaries,  
 310 our criterion for selecting data in different nation-regions is rather simple and based  
 311 upon a similar criterion used in recent NGA-West2 GMPEs, e.g., Abrahamson et al.  
 312 (2014) and Boore et al. (2014). The  $t^*$ -R data for the three region categories is plotted  
 313 in Figure 3. As can be noted from Figure 3, the majority of the data belongs to Turkey  
 314 with 667 data points, followed by 372 from Italy and the remaining 161. Out of the  
 315 three, only data from Turkey shows a uniform distribution with distance, the data from  
 316 Italy and remaining stations is mostly concentrated at less than 70-80 km. Similar to  
 317 Figure 2, the  $t^*$ -R data is binned in 10 km distance bins and corresponding median  
 318 values and spread in each bin is also plotted over the actual distribution of the data.  
 319 Although, one may observe a distance dependent variation in slope, a straight line fit  
 320 over  $t^*$ -R data from Turkey captures the observed trend reasonably well. The Italian  
 321 data is mostly concentrated at smaller distances. Nevertheless, the straight line fit  
 322 captures the observed trend well over the full distance range. Due to the very limited  
 323 data points beyond 80 km, the fit was performed only up to 80 km for the remaining  
 324  $t^*$ -R data (Figure 3c). It is worth mentioning that, the fitted lines shown in Figure 3 are  
 325 obtained from the fitting of actual data points. Using  $\beta = 3.5$  km, the  $Q_0$  values and  
 326 associated variabilities for the three region categories are shown in Figure 4a. Figures 3  
 327 and 4a clearly indicate that within the selected dataset and at large in the RESORCE  
 328 database, there are strong regional variations in anelastic attenuation. The data from

329 Turkey exhibits rather low attenuation (high  $Q_0$ ) in comparison to that for Italy, an  
 330 observation that was also noted by Boore et al. (2014) and Kotha et al. (2016) in their  
 331 empirical models.

332 Estimation of  $\kappa_0$  using equation (3) is strongly biased upon the assumed  $Q$  model.  
 333 Consequently, and as can also be observed in Figure 4b, a higher  $Q_0$  gives a higher  $\kappa_0$   
 334 and similarly lower  $\kappa_0$  is obtained for a lower  $Q_0$ . A smaller variability in  $Q_0$  and  $\kappa_0$   
 335 (Figure 4b) for Italy in comparison to that for Turkey can be attributed to that the  
 336 Italian dataset is mainly concentrated at smaller distances. Hence, the ray paths are  
 337 mostly sampling similar (shallower) depths in the subsurface, thus fewer variations due  
 338 to anelastic attenuation. For the remaining dataset, the large uncertainty can be  
 339 explained due to its regional heterogeneity. Therefore, depth variations in  $Q_0$  can be  
 340 expected as well as the regional variations. In order to further investigate the regional  
 341 variations in  $\kappa_0$ , we constrained  $Q_0$  from the common (database) bilinear model shown  
 342 in Figure 2a to estimate the average  $\kappa_0$  in Turkey and Italy. Additionally, we limit the  
 343 data only up to 50 km for this analysis to constrain the bias from  $Q_0$  variations. As  
 344 expected due to the coupling of  $Q_0$  and  $\kappa_0$ , one can observe in Figure 4b that the  $\kappa_0$   
 345 values are different than that when we use regional  $Q_0$  values (Figure 4a) for Turkey  
 346 and Italy. However, the rather important observation is that using a common  $Q_0$  value  
 347 for the two regional datasets also indicates a significant variation in attenuation  
 348 properties for Turkey and Italy due to surficial layers as near distance earthquakes are  
 349 expected to sample near-surface structure of the subsurface. Hereafter, regional  $Q_0$   
 350 values for Turkey and Italy will be used for further analysis. While for the remaining  
 351 dataset the database based distance-dependent  $Q_0$  model (Figure 2a) will be used.

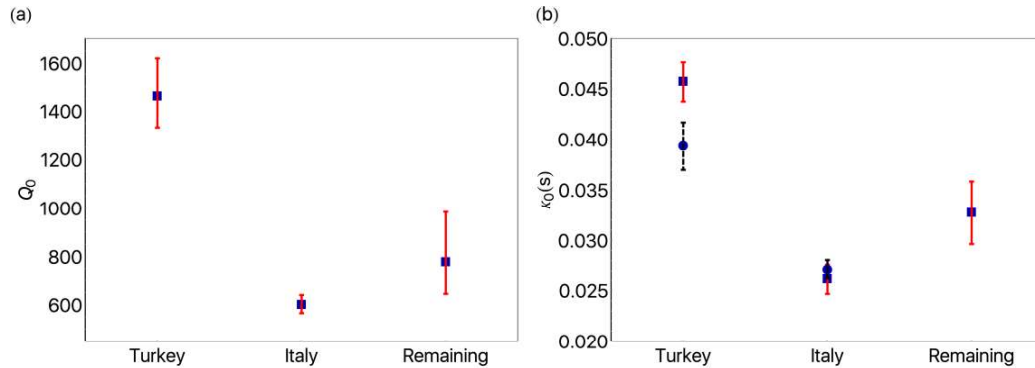


352  
 353 **Figure 3.**  $t^*$ -distance model for: (a) Turkey, (b) Italy, (c) and remaining dataset. Empty circles indicate individual  
 354 data points while empty squares represent the median of  $t^*$ - $R$  data in each 10 km distance bin, while the extent of  
 355 vertical bars indicates the  $t^*$  values corresponding to 16 and 84 percentiles in the bins.

### 356 5. Station and site-class specific $\kappa_0$

357 In stochastic simulations (Boore 2003) as well as HTTA adjustments of empirical  
 358 GMPEs a prior measurement of  $\kappa_0$  at a given site is required (e.g., Campbell 2003;

359 Van Houtte et al. 2011; Edwards et al. 2016). In order to obtain a station-specific  $\kappa_0$   
 360 estimate, we correct all the individual record  $t^*$  (both the components individually) for  
 361 the slope in  $t^*-R$  straight-line fit corresponding to regional  $Q_0$  values, that is, 1462 for  
 362 Turkey and 601 for Italy. For the remaining dataset, the database based, the two-slope  
 363  $t^*-R$  model presented in Figure 2a is used. Subsequently, the median of all record  $\kappa_0$   
 364 values at a station is presented as the station  $\kappa_0$ . Table 1 presents estimated  $\kappa_0$  values  
 365 for 45 stations recording at least 14 component-records.

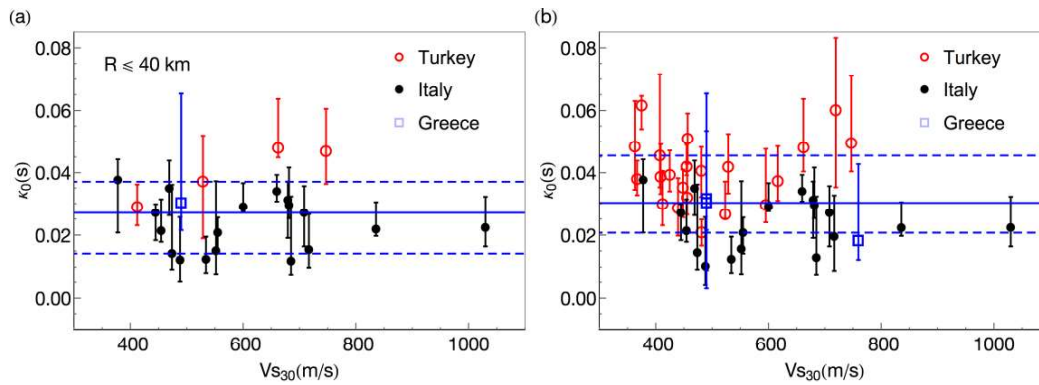


366

367 **Figure 4.** Regional variations in inelastic attenuation parameter  $Q_0$  (a) and site-related attenuation  $\kappa_0$  (b). The  
 368 squares in (b) indicate average  $\kappa_0$  values when the respective  $Q_0$  values of (a) are used while the discs indicate the  
 369  $\kappa_0$  values when the database based bilinear  $Q_0$  model shown in Figure 2a is used. The extent of the vertical bars  
 370 corresponds to the 68% confidence interval of each parameter estimate.

371 Figure 5 depicts variation of station  $\kappa_0$ , and associated variability with  $V_{S30}$  for  
 372 stations with  $V_{S30} > 360$  m/s and with minimum ten records (including both the  
 373 components). Figure 5a depicts the plot only for stations that have recorded  
 374 earthquakes located at a distance  $\leq 40$  km. As mentioned earlier, regional variation in  
 375  $Q$  models can bias the estimation of  $\kappa_0$ ; thus Turkish stations are observed to exhibit  
 376 consistently higher  $\kappa_0$ . An important observation from Figure 5 is that, there is a rather  
 377 large record-to-record (within-station) variability (the vertical bars) in  $\kappa_0$ , which in  
 378 many cases is comparable to the station-to-station (between-station) variability  
 379 (horizontal dashed-lines) of  $\kappa_0$ . The between-station variability is mainly affected by  
 380 regional variations in  $Q_0$ . Although we did not observe a clear correlation between  $\kappa_0$   
 381 and  $V_{S30}$  (Figure 5b), the between-station variability can also increase since softer sites  
 382 may exhibit higher  $\kappa_0$  (Chandler et al. 2006; Van Houtte et al. 2011; Edwards and Fäh  
 383 2013a). On the other hand, the within-station variability is due to the fact that  $Q_0$  is not  
 384 homogeneous with respect to depth (Edwards et al. 2008; Edwards et al. 2011). Hence  
 385 estimating  $\kappa_0$  from near as well as distant earthquakes using a homogenous  $Q$  model

386 can also inflate the within-station variability. As can also be noted from Figure 5b: the  
 387 Italian stations depict less within-station variability in comparison to the Turkish  
 388 stations. Additionally, a possible source component in  $\kappa_0$  (Kilb et al. 2012) can also  
 389 contribute to the larger within-station variability. Figure 6 demonstrates the effect of  
 390 within-station variability in  $\kappa_0$  by showing plots of spectra obtained from actual fit and  
 391 that from regional  $Q_0$  and station  $\kappa_0$ , vis-à-vis observed spectra. The spectra are shown  
 392 at a station in Turkey with  $V_{S30} = 747$  m/s and for earthquakes at less than 40 km  
 393 distance from the station.

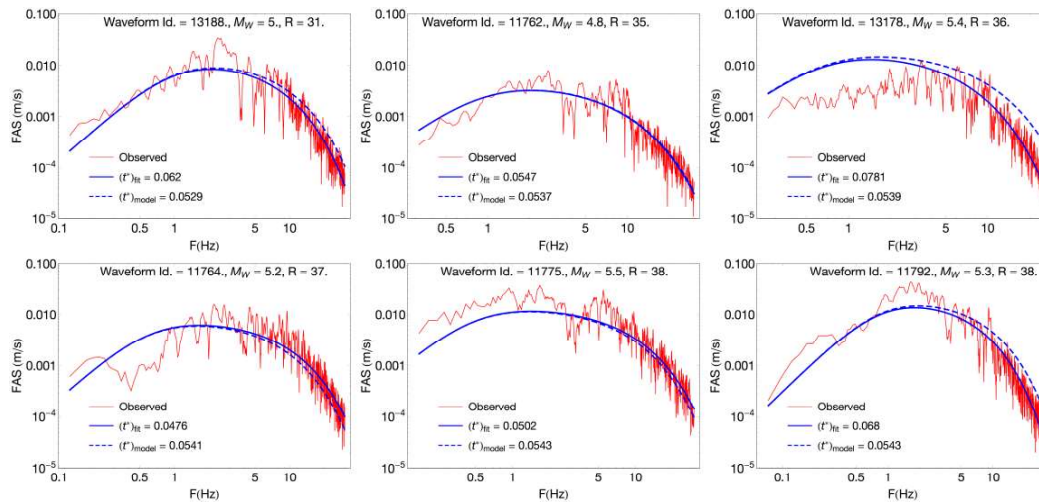


394

395 **Figure 5.** Station  $\kappa_0$  plotted against  $V_{S30}$  values for  $V_{S30} > 360$  m/s: (a) when earthquakes located at less than 40  
 396 km (from a station) are used; (b) when all the earthquakes recorded at a station are used. Markers (empty circles,  
 397 disks and empty squares) indicate the median while the extent of vertical bars indicates the values corresponding  
 398 to 16 and 84 percentiles at each station, i.e., within-station variability. The horizontal solid line indicates the median  
 399 value of all station  $\kappa_0$  in the sample, while two dashed lines indicate 16 and 84 percentile values in the sample, i.e.  
 400 between-station variability. In both cases stations which have recorded at least 10 records (including both the  
 401 components) are used.

402 In order to cover a broad range of station sites, we also estimate site class specific  $\kappa_0$   
 403 values, which can be used as a first order approximation for stations not having  
 404 endemic measurements of  $\kappa_0$ . In addition to the regional classification based upon  $Q_0$ ,  
 405 stations were classified in different site-classes based upon their  $V_{S30}$  values as: very  
 406 soft soil as  $V_{S30} \leq 180$  m/s,  $180 < V_{S30} \leq 360$  m/s as soft soil,  $360 < V_{S30} \leq 750$  m/s as  
 407 stiff soil and  $V_{S30} > 750$  m/s as rock sites. Subsequently the site class  $\kappa_0$ , in each  
 408 regional subset, is computed as the median of all record  $\kappa_0$ . The site class specific  $\kappa_0$   
 409 and corresponding variabilities are presented in Table 2. A rather large  $\kappa_0$  for rock  
 410 sites in Turkey can be a sampling issue with only eight data points. For Italian sites we  
 411 observe a decreasing  $\kappa_0$  from very soft soil sites to rock sites. In the remaining dataset,  
 412 there were no stations corresponding to the very soft soil site condition. For a  
 413 combined (data from all regions), but significantly limited subset of this dataset,  
 414 Edwards and Fäh (2013a) obtained  $\kappa_0$  as 0.0326, 0.0375, 0.0303 and 0.0241s for very  
 415 soft soil, soft soil and stiff soil and rock site respectively. The values of site class  $\kappa_0$

416 for Turkish dataset from this study are comparable with the findings of Askan et al.  
 417 (2014) with  $\kappa_0$  values 0.0377 and 0.0455 s in stiff and soft soil category.  
 418



419  
 420 **Figure 6** Within station variability of  $\kappa_0$ . Spectra for acceleration traces recorded at a station (Stn. Id. 2322) in  
 421 Turkey with a  $V_{S30}$  of 747 m/s. The regional  $Q_0$  1462 for Turkey is used along with the station  $\kappa_0$  0.0468s.

422

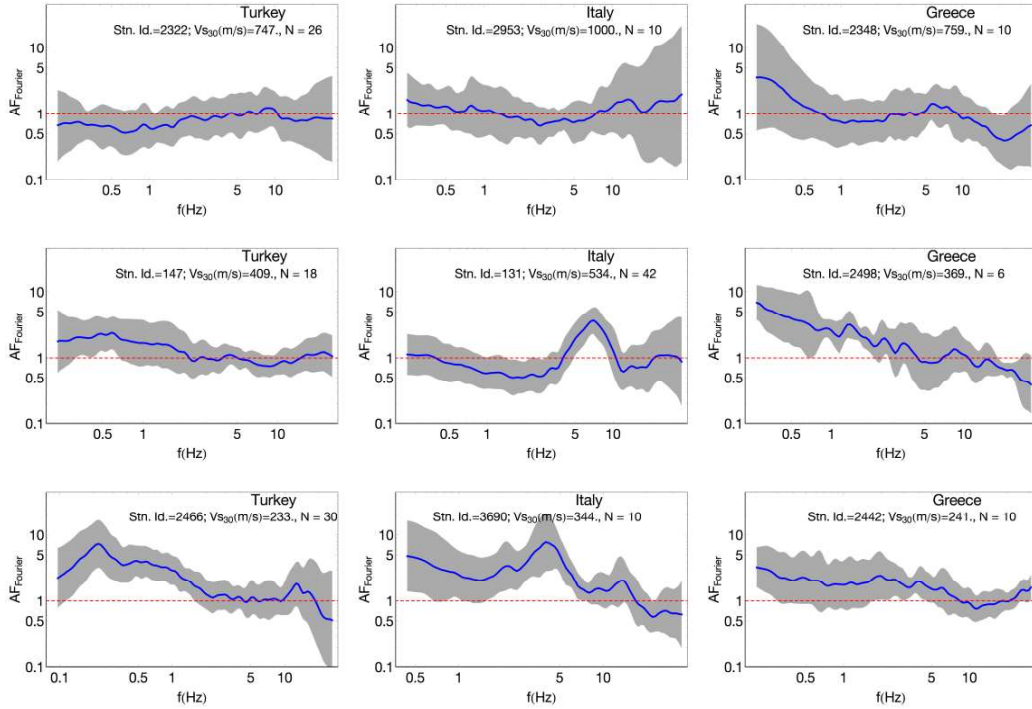
## 423 6. Station and site-specific amplification

424 We invert for a reference model using *a priori* seismic moments and geometrical  
 425 spreading from Bora et al. (2015). The station (Fourier) site amplification factors  
 426 ( $AF_{\text{Fourier}}$ ) are estimated with respect to this reference model from a residuals analysis  
 427 (Edwards et al. 2008; Drouet et al. 2010; Edwards and Fäh 2013a). For the reference  
 428 model,  $M_0$  is used from database  $M_W$  and  $t^*$  values were fixed to a value that is  
 429 obtained from a combination of regional  $Q_0$  and station  $\kappa_0$  derived in the previous  
 430 section. In order to obtain the site  $AF_{\text{Fourier}}$  at one station, we take mean of all (log)  
 431 residuals (at each frequency) with respect to the reference model. Out of total 350, only  
 432 223 stations characterized with measured  $V_{S30}$  estimates are used in the site  
 433 amplification analysis.

434 Figure 7 depicts  $AF_{\text{Fourier}}$  plots for selected stations, which have recorded at least ten  
 435 horizontal records (five earthquakes), except for a station (station Id. 2498) in Greece.  
 436 Stations with station Ids 131 and 3690 indicate resonance effects present at such sites,  
 437 which are consistent with the notion that stiff soil/rock sites may indicate resonance  
 438 peaks at high frequencies while at softer soil sites such effects are mostly dominant at  
 439 lower frequencies. It is worth to note here that, for determining  $AF_{\text{Fourier}}$ , we  
 440 additionally excluded the records recorded at  $R \leq 60$  km (from earthquakes with



441  $M_W \geq 6.5$ ) to avoid the nonlinear soil response effects. Consistent with our site-class  
442 specific  $\kappa_0$  estimates, we also present site-class specific amplification factors  $AF_{\text{Fourier}}$   
443 for the four site classes for each regional subset in Figure 8. Such plots also provide  
444 guidance in defining the amplification at stations for which direct measurements of  $V_S$ -  
445 profiles are not available. Although, resonance peaks are not apparent in the site-class  
446  $AF_{\text{Fourier}}$  curves due to the broad site classification, the very soft and soft soil site  
447 indicate a large amplification at lower frequencies, and a deamplification at large  
448 frequencies may indicate (residual) non-linear site effects. Whereas, the stiff soil and  
449 rock sites indicate amplifications almost independent of frequency. Regional variations  
450 in site-class average site amplification factors are not apparent from Figure 8. Rock  
451 motions show an amplification close to one, which indicates that the reference is well  
452 calibrated. Also, the overall slight-deamplification for rock ( $V_{S30} > 750$  m/s) in  
453 Turkey is consistent with respect to the chosen reference amplification of California  
454 (Boore and Joyner 1997) anchored at  $V_{S30}$  620 m/s. However, the similar  $AF_{\text{Fourier}}$   
455 curves for stiff soil and rock conditions in Italy indicate towards misclassification for  
456 some of the stations (Lucia Luzi, *personal communication*). It is worth emphasizing  
457 again that these amplification curves are obtained with respect to a crustal reference  
458 amplification of Boore and Joyner (1997) by removing it from the observed spectra.  
459 Therefore, Boore and Joyner (1997) crustal amplification curve should be used along  
460 with these  $AF_{\text{Fourier}}$  curves in a forward prediction application.



461

462

463

464

**Figure 7.** Station-specific Fourier amplification curves for selected stations. The thick curve indicates means amplification and the gray shaded bands indicate extent of the standard deviation. It may be noted that the site amplification curves are presented only for the stations, which are characterized by a measured  $Vs_{30}$  estimate.

465

466

## 7. Source parameters $M_W$ and $\Delta\sigma$

467

468

469

470

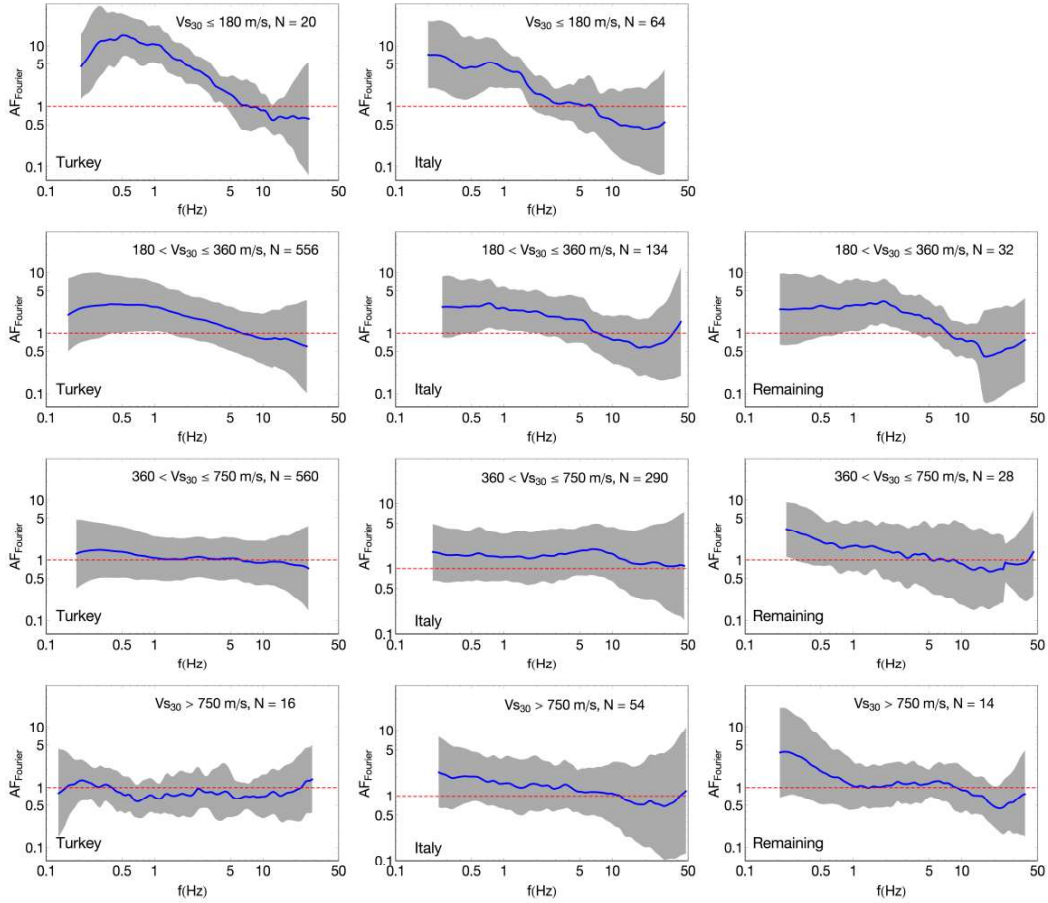
471

472

473

474

After estimating the site amplification curves,  $AF_{\text{Fourier}}$ , we refit the site-corrected spectra to determine event-specific  $f_c$  as well as seismic moments. We use site-class specific  $AF_{\text{Fourier}}$  curves (Figure 8) to correct the observed spectra for site amplification effects. The site-class  $AF_{\text{Fourier}}$  curves represents the site amplification effects over a broad range of stations; hence obviously they may not capture the detailed amplification characteristics of a single station, rather reflecting a typical feature. Nevertheless, they allow including the stations, which have recorded fewer earthquakes and also limiting the bias due to those fewer recordings.



475  
476  
477

**Figure 8.** Region-wise site class-specific Fourier amplification. The thick curve indicates the mean amplification and the gray shaded bands indicate the extent of one standard deviation.

478 In this iteration, other than the geometrical spreading function, the high frequency  
479 slope  $t^*$  is fixed to the value that is a combination of regional  $Q_0$  models and a regional  
480 site-class  $\kappa_0$  (Table 2). The fitting is focused to fit the low frequency spectral level of  
481 the acceleration spectrum, i.e.,  $f \leq 10$  Hz. In order to avoid the trade-off between  $M_W$   
482 (magnitude) and  $\Delta\sigma$  at frequencies beyond  $f_c$ , we do not include the high frequency  
483 spectral amplitudes in fitting at this stage. The choice of 10 Hz is rather subjective and  
484 is based on the assumption that this can be the highest  $f_c$  in the dataset as most of the  
485 earthquakes are of low-to-moderate magnitudes ( $M \geq 4$ ). In Brune's (1970,1971)  
486 source model for far-field spectrum of displacement motion, the spectral amplitude  $Y$   
487 (plateau) below  $f_c$  is related to  $M_0$  as:

$$488 \quad Y(f \ll f_c) = \frac{M_0 \xi \theta F}{4\pi \beta^3 \rho}. \quad (5)$$

489 In equation (5), the values, of near source density ( $\rho$ ), near source average shear wave  
490 velocity ( $\beta$ ), average radiation coefficient for  $S_H$  waves ( $\theta$ ), energy partition  
491 coefficient ( $\xi$ ) and free surface amplification factor ( $F$ ) remain the same as used in

492 equation (1). The estimated  $M_0$  is used to compute the inverted magnitude  $M_W$  using  
 493 the Hanks and Kanamori (1979) relation. Almost 1:1 correlation can be observed  
 494 between database and inverted  $M_W$  in Figure 9. However, the over prediction of  $M_W$   
 495 values from uncorrected spectra illustrates the challenge in estimating  $M_W$  values from  
 496 observed Fourier spectra in presence of significant site-effects.

497 The inverted  $f_c$  and  $M_W$  are used to compute the stress parameters ( $\Delta\sigma$ ) using the  
 498 following relationship:

$$499 \quad \Delta\sigma = M_0 \left( \frac{f_c}{0.4906\beta} \right) \quad (6)$$

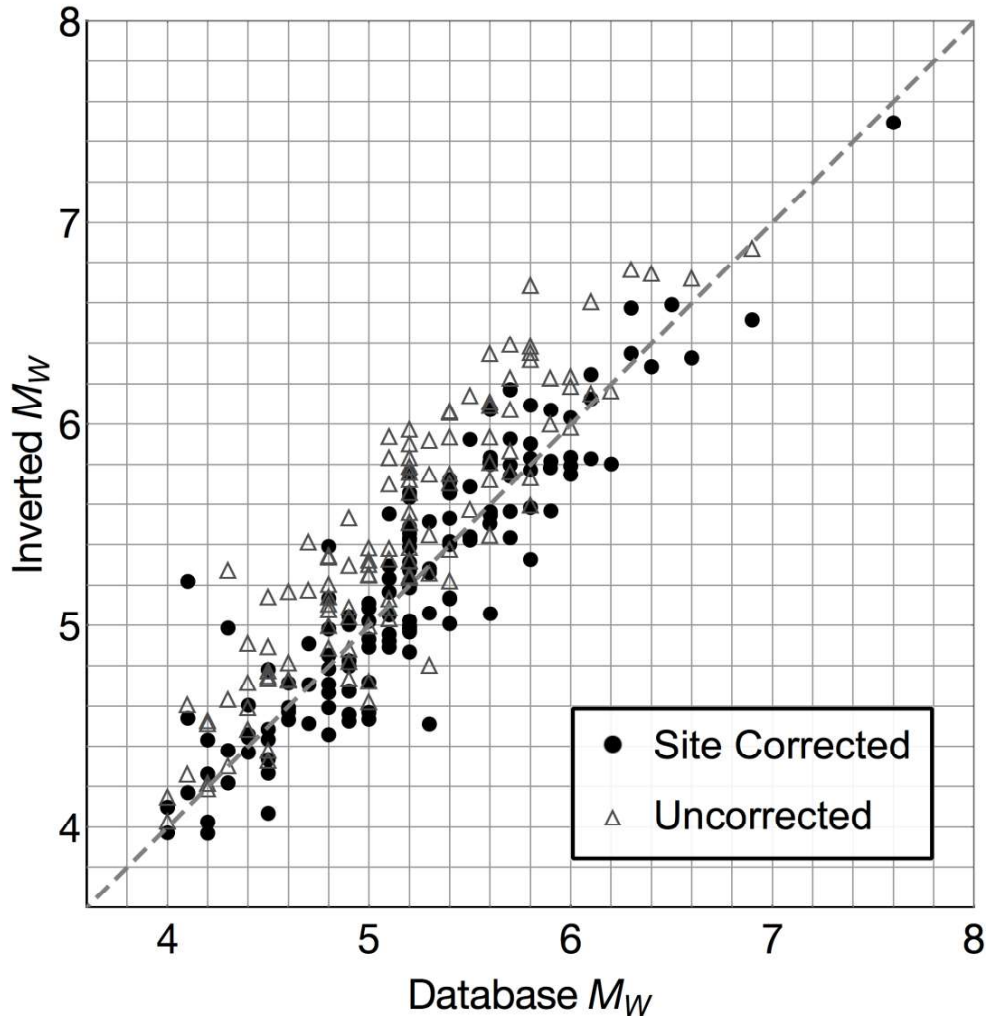
500 (Brune 1970, 1971; Eshelby 1957) where  $\beta$  is the near-source shear wave velocity  
 501 assumed to be 3500 m/s. Figure 10a depicts the variation of  $\Delta\sigma$  values with respect to  
 502 database  $M_W$  and Figure 10b illustrates the same variation with focal depth. To obtain  
 503 a robust estimate of inverted  $f_c$  and  $M_W$ , events recorded on at least three stations are  
 504 used for this analysis. As found for the previous database (Edwards and Fäh 2013a)  
 505 Figure 10a does not show any magnitude dependency of  $\Delta\sigma$ . Thus, assuming a  
 506 constant  $\Delta\sigma$  model, the  $\Delta\sigma$  (in MPa) using inverted  $M_W$  is obtained as:

$$507 \quad \log_{10} \Delta\sigma = \log_{10} 5.75 \pm 0.43. \quad (7)$$

508 If we constrain  $M_0$  to a value from database  $M_W$  and invert for  $f_c$  only, the median  $\Delta\sigma$   
 509 is obtained identical to that in equation (7) with smaller (lognormal) standard deviation  
 510 as:

$$511 \quad \log_{10} \Delta\sigma = \log_{10} 5.65 \pm 0.33 \quad (8)$$

512 The median  $\Delta\sigma$  values are slightly smaller than those obtained by Edwards and Fäh  
 513 (2013a) as 8.8 and 7.4 MPa from inverted and database  $M_W$  respectively, while the  
 514 standard deviations are comparable. The  $\Delta\sigma$  variability obtained in this study is also  
 515 comparable with that inferred (Cotton et al. 2013) from between-event variability in  
 516 the GMPEs of Akkar et al. (2014a), Boore et al. (2014) and Bindi et al. (2014) as: 0.43,  
 517 0.42 and 0.41 respectively.



518  
519  
520  
521  
522

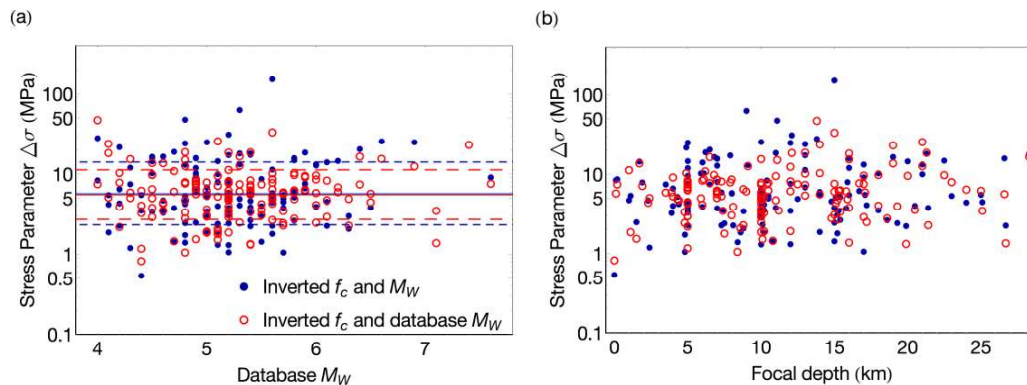
**Figure 9.** Comparison of inverted  $M_W$  with that from database. Disks: when inverted  $M_W$  are obtained from site-class specific amplification corrected; and empty triangles: when inverted  $M_W$  are obtained from uncorrected spectra. Events that have been recorded at least at three stations (six records including both the components) are shown.

523

524 Additionally, we estimated  $\Delta\sigma$  for the  $M_W$  4.8 St. Die earthquake, as it has been widely  
525 investigated and discussed in the literature (e.g., Scherbaum et al. 2004). Although, the  
526 station-specific  $V_{s30}$  values are not available for the stations recording St. Die  
527 earthquake, the soil type information of those stations was obtained from RESIF  
528 seismic data portal (<http://seismology.resif.fr/>). Out of the nine stations, three stations  
529 were classified in the EC (Eurocode)-8 soil type E, two in soil type B and the  
530 remaining four were classified in soil type A. We did not apply any corrections to  
531 empirical Fourier spectra to account for the local site amplification effects except  
532 correcting for the crustal amplification related with the generic rock amplification of  
533 California (Boore and Joyner 1997). However, the  $t^*$  values were fixed using the two

534 separate  $\kappa$  (or  $t^*$ ) models (i.e., for soil and rock) of Douglas et al. (2010), as some of  
 535 the stations (which recorded St. Die earthquake) are included in their analysis as well.  
 536 Fixing the low frequency spectral level by the  $M_0$  obtained from database  $M_W$  gives  
 537 the  $\Delta\sigma$  value as 49.2 MPa, while inverting for both  $f_c$  and ( $M_0$ ) magnitude gives  $\Delta\sigma$  as  
 538 32.3 MPa corresponding to the fitted  $M_W$  4.96. Such high values are consistent with  
 539 high ground motion amplitudes observed for this event.

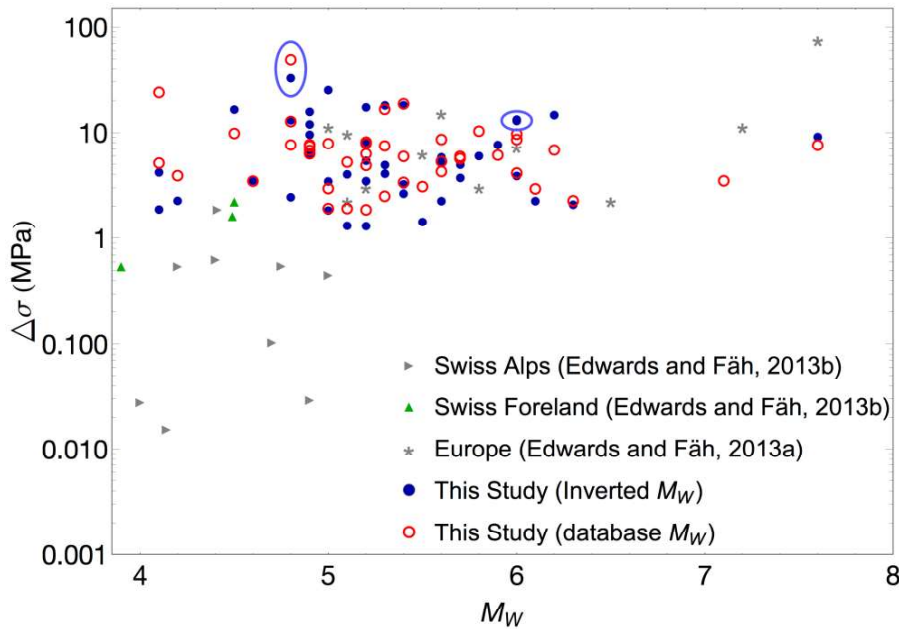
540 The values of  $\Delta\sigma$  determined in this study are compared in the context of recent studies  
 541 involving  $\Delta\sigma$  determination for mainland Europe (Edwards and Fäh 2013a; Edwards  
 542 and Fäh 2013b) in Figure 11. Edwards and Fäh (2013a) involves earthquakes from all  
 543 over Europe and the Mediterranean, which is essentially a subset of the present dataset,  
 544 while the analysis of Edwards and Fäh (2013b) is based upon the earthquake from  
 545 Swiss Alps and Swiss Foreland basin.  $\Delta\sigma$  values from present study are observed to be  
 546 in good comparison to the other studies except that the earthquakes from Swiss Alps  
 547 are exhibiting lower  $\Delta\sigma$  values.



548  
 549 **Figure 10.** Stress parameters ( $\Delta\sigma$ ) (obtained from site-class specific amplification corrected spectra) plotted  
 550 against database  $M_W$  in panel (a) against depth in panel (b). Disks indicate the  $\Delta\sigma$  values when both  $f_c$  and  $M_W$   
 551 were obtained from inversion while the empty circles indicate those when only  $f_c$  was obtained from inversion  
 552 keeping the  $M_0$  fixed from database  $M_W$ . Again, events recorded at least at three stations (six records including  
 553 both the components) are shown.

554 Apart from St. Die earthquake, that is exhibiting a relatively larger  $\Delta\sigma$ , we did not  
 555 observe discernable regional pattern in  $\Delta\sigma$  (from the present dataset) as suggested by  
 556 some recent studies (Malagnini et al. 2008; Drouet et al. 2010; Yenier and Atkinson  
 557 2015b; Goertz-Allmann and Edwards 2014). The Friuli earthquake  $M_W$  6, 1976 also  
 558 indicates a large  $\Delta\sigma$  of 13.38 MPa with inverted  $M_W$  5.79, while using the database  
 559  $M_W$  gives  $\Delta\sigma$  as 8.6 MPa. In Figure 11, earthquakes recorded at least at seven stations  
 560 (fourteen records including both the components) are shown. For the earthquakes

561 shown in Figure 11, inverted  $f_c$ ,  $M_W$ ,  $\Delta\sigma$  and the associated uncertainties are given in  
 562 Table 3.



563

564 **Figure 11.**  $\Delta\sigma$  comparison with the previous studies from the same region. Events recorded at least at seven  
 565 stations (fourteen records including both the components) are shown in this figure. The encircled markers indicate  
 566 the  $\Delta\sigma$  values (left and right) corresponding to St. Die and Friuli earthquakes respectively.

567

## 568 8. Discussion

569 From the present analysis, we observed regional variations in anelastic attenuation  $Q_0$   
 570 and  $\kappa_0$  from shallow active crustal earthquakes recorded across Europe and  
 571 Mediterranean. Although, estimation of  $\kappa_0$  is strongly linked with how one constrains  
 572  $Q_0$ , our analysis also indicates that it may also vary significantly between Turkey and  
 573 Italy. As some studies have investigated correlation of  $\kappa_0$  with deeper structure  
 574 (Campbell 2009; Ktenidou et al. 2015), there is a possibility that  $\kappa_0$  has regional  
 575 component (Ktenidou et al., 2015), which depends on varying crustal properties.

576 Furthermore, within a single region, significant, record-to-record (within-station)  
 577 variability in  $\kappa_0$  is observed, which in many cases is comparable to the station-to-  
 578 station (between-station) variability. Large within-station variability can be expected  
 579 when a station records earthquakes over a range of distances. Thus the waves reaching  
 580 at the station may encounter different anelastic attenuation regimes due to sampling  
 581 deeper layers as well as the shallower layers in the subsurface. Essentially this  
 582 variability is entering in  $\kappa_0$  through the depth variation of  $Q_0$ . For the estimation of  $\kappa_0$

583 therefore it is recommended to use records from near station earthquakes in addition to  
584 account for regional differences in  $Q_0$ . Large within-station variability in  $\kappa_0$  can also  
585 be contributed by the source-component present in  $\kappa_0$  (Kilb et al. 2012). From an  
586 application perspective, for example in stochastic simulations and HTTA adjustment of  
587 GMPEs, a linked (or combined)  $Q$  and  $\kappa_0$  model should be used to maintain the  
588 consistency. Finally, an important consequence of larger within-station variability (in  
589  $\kappa_0$ ) from the GMPE adjustment perspective is that it can hinder the effect of site  
590 (station) corrections made in  $\kappa_0$  to account for site-to-site variability. This article  
591 presents broad site-class based  $\kappa_0$  measurements for the regional subsets as well as the  
592 station-specific  $\kappa_0$ . We did not observe a clear relationship between  $\kappa_0$  and  $V_{S30}$  as  
593 suggested by some other studies.

### 594 **8.1 Comparison with previous studies**

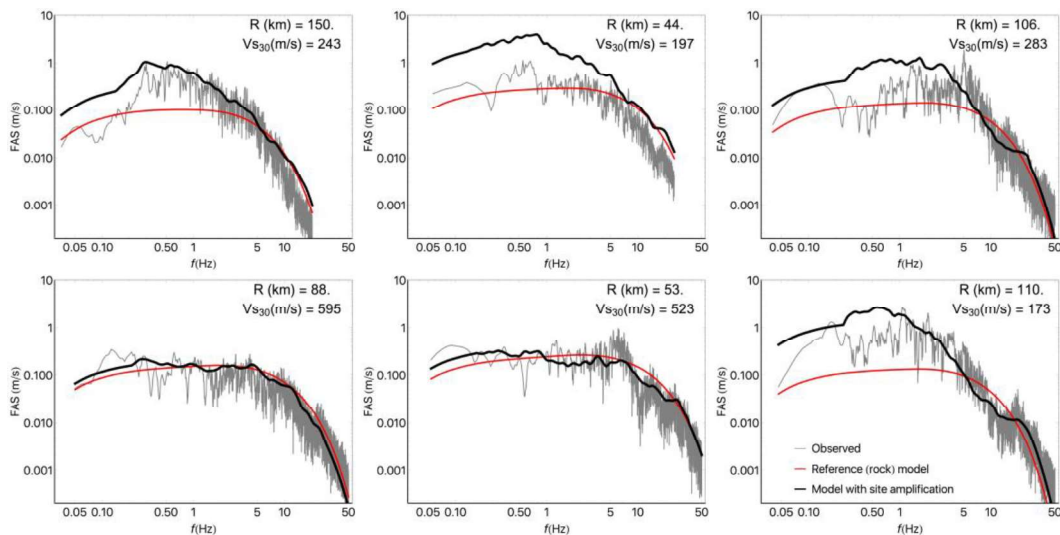
595 A meaningful comparison between the estimated parameters with previous studies can  
596 only be possible when underlying assumptions (e.g., mainly geometrical spreading)  
597 and method of estimation is the same amongst the studies. Nevertheless, anelastic  
598 attenuation  $Q$ ,  $\Delta\sigma$  and  $\kappa_0$  for different regions across Europe and Mediterranean from  
599 some representative studies are given in Table 4 along with the assumed geometrical  
600 spreading function. To facilitate comparison with a frequency-independent  $Q_0$  from  
601 our study, we have fixed  $Q$  at 10 Hz from the studies involving frequency dependent  
602  $Q$ . As expected a significant variation amongst the studies can be seen in Table 4. The  
603  $Q_0$  values determined in this study agree with the general trend that Turkey and Greece  
604 exhibit higher  $Q$  values (lower attenuation) in comparison to that in Italy. Our  $Q_0$   
605 estimates for Turkey are consistent with the findings for the northwestern part  
606 (Kurtulmus and Akyol 2013; Askan et al. 2014), which is expected as the majority of  
607 our Turkish records come from this region. Similarly, the  $\kappa_0$  value for Turkey from our  
608 study is in good agreement with the value of 0.045s found by Akinici et al. (2013) for  
609 Anatolian region in Turkey. Moreover, recent GMPEs (Boore et al. 2014; Kotha et al.  
610 2016; Kuehn and Scherbaum 2016) have also indicated regionally varying anelastic  
611 attenuation terms indicating a higher  $Q$  in Turkey and lower  $Q$  in Italy. The present  
612 dataset does not permit to investigate regional variations in  $\Delta\sigma$ . The average median  
613  $\Delta\sigma$  value of 5.65 MPa from our analysis for the entire region is broadly consistent with  
614 the previous studies, except with the very high values of 20 and 60 MPa from Umbria-  
615 Marche and northeastern regions in Italy (Malagnini and Herrmann 2000; Malagnini et



616 al. 2002). However, as stated earlier, comparisons amongst the parameter estimates  
 617 should be made relative to the geometrical spreading function rather than treating them  
 618 as absolute values.

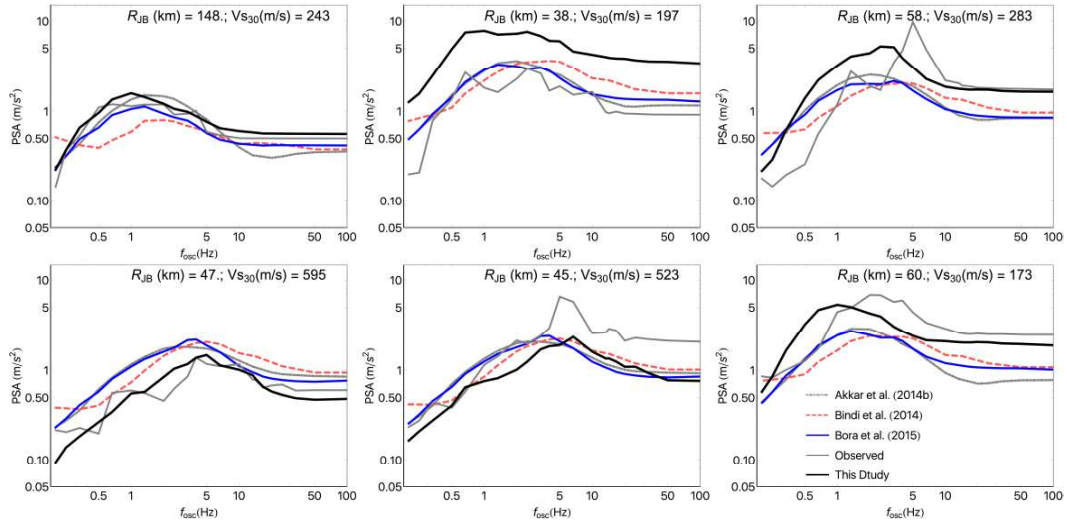
## 619 **8.2 Stochastic model predictions**

620 We validate the model parameters derived in this study by comparing the model  
 621 predictions against recorded data. The comparison is performed in terms of graphical  
 622 comparisons of Fourier and response spectra in figures 12 and 13 respectively, while  
 623 Figure 14 depicts comparison of response spectral variability with the regional  
 624 GMPEs. For graphical comparison in figures 12 and 13, we have chosen August 17,  
 625 1999 Kocaeli earthquake  $M_W$  7.6. This choice of earthquake will also allow reader to  
 626 appreciate the consistency of the point source model in simulating ground motions  
 627 from rather large ruptures. In addition to the use in synthesizing ground motions for  
 628 low seismicity regions the model parameters such as  $\Delta\sigma$ , geometrical spreading,  $Q$  and  
 629  $\kappa_0$  are also used to represent the source, path and site attributes of empirical GMPEs in  
 630 their HTTA (Host-to-Target Adjustment) framework. To that end, as depicted in  
 631 Figure 13, a good comparison of the response spectra obtained from our stochastic  
 632 model with the regional GMPEs of Akkar et al. (2014b), Bora et al. (2015) and Bindi  
 633 et al. (2014) warrants the use of the present model in such exercises.



634

635 **Figure 12.** Example of Fourier spectral fits to the observed recordings from  $M_W$  7.6 Kocaeli earthquake (August  
 636 17, 1999). The model predictions (heavy line) are shown for inverted  $M_W$  7.5,  $\Delta\sigma = 9.1$  MPa and station-specific  
 637  $\kappa_0$  and amplifications.



638

639

640

**Figure 13.** Pseudo spectral acceleration (PSA) for Kocaeli records corresponding to the plots shown in Figure 12. PSA from Akkar et al. (2014b), Bindi et al. (2014) and Bora et al. (2015) are also shown for comparison.

641

642

643

644

645

646

647

648

649

650

651

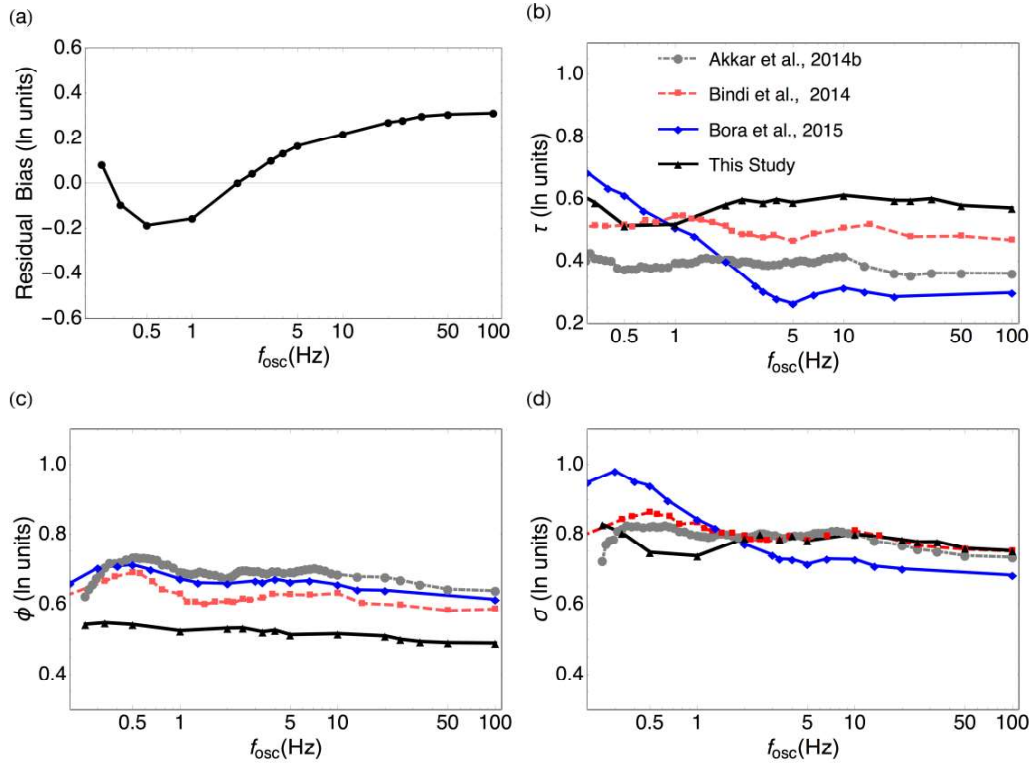
652

653

654

655

Figure 14 depicts comparison of response spectral variability obtained from the present stochastic model with the regional empirical models (Akkar et al. 2014b; Bindi et al. 2014; Bora et al., 2015). Response spectral residuals were obtained for an average  $\Delta\sigma = 5.65$  MPa and site amplification curves for the stations recording at least four component-records, with measured  $Vs_{30}$  measurements along with the regional  $Q_0$  and corresponding station-specific  $\kappa_0$  values. The residuals were decomposed into between- and within-event components by performing a linear (intercept-only) mixed-effects regression (*lme4* package, Bates et al. 2015) on the total residuals. Figure 14a depicts the mean residual bias at each oscillator frequency; Figure 14b depicts between-event standard deviation ( $\tau$ ); figure 14c depicts within-event standard deviation ( $\Phi$ ) and Figure 14d depicts the total standard deviation ( $\sigma$ ). Significant reduction in within-event variability ( $\Phi$ ) is mainly due to capturing the between-station variability in terms of site amplification and  $\kappa_0$  in the model itself. Also, capturing the regional variability in  $Q_0$  has also led to further reduction in  $\Phi$ .



656

657 **Figure 14.** Comparison of response spectral variability from the derived stochastic model (using median  $\Delta\sigma = 5.65$   
658 MPa, regional Q along with station-specific  $\kappa_0$  and amplifications) with that from regional empirical models. (a)  
659 Residual bias; (b) between-event variability ( $\tau$ ); (c) within-event variability ( $\Phi$ ); (d) total variability ( $\sigma$ ). The  
660 variability from Bora et al. (2015) corresponds to the curve (in their Figure 17) that is obtained with event-specific  
661  $\Delta\sigma$  and station-specific  $\kappa_0$ .

## 662 9. Conclusions

663 This study was aimed at providing measurements of regional source, attenuation and  
664 site parameters for Europe and the Mediterranean region based upon a subset-dataset  
665 (Bora et al. 2015) of RESORCE-2012 database. Estimation of source, path and site  
666 parameters is based upon the far-field spectral representation of strong ground motion  
667 phases. In which, the source is represented by a Brune (1970, 1971) single corner  
668 frequency ( $f_c$ ) model. The path effects are modeled using simple geometrical and  
669 inelastic attenuation models. The inelastic attenuation is parameterized in terms of a  
670 frequency-independent  $Q_0$  model (Edwards et al. 2008; Campbell 2009; Edwards and  
671 F  h 2013a). As detailed in Bora et al. (2015), to enable the validity of point source  
672 model, near distance records from moderate and large magnitude earthquakes have  
673 been discarded. In the first stage, we fit for source-corner frequency  $f_c$  and attenuation  
674 operator  $t^*$  by fixing the  $M_0$  to a value obtained from database  $M_W$  (Hanks and  
675 Kanamori 1979).

676 The inverted  $t^*$  values from the full dataset indicate a  $Q_0$  model varying with distance  
677 that essentially captures depth-dependent  $Q$  structure (Edwards et al. 2008, Edwards et  
678 al. 2011). However, a clear regional variation in inelastic attenuation ( $Q_0$ ) is observed  
679 with a large value of  $Q_0$ , i.e., 1462 (smaller attenuation) for Turkey and smaller  $Q_0$   
680 (larger attenuation) of 601 for Italy. We also investigated  $\kappa_0$  variability in terms of  
681 between-station and within-station (record-to-record) components indicating a large  
682 contribution in within-station variability through regional and depth variations of  $Q$ .  
683 Station-specific average Fourier site amplification factors were obtained with respect  
684 to a reference site with shear wave velocity ( $V_s$ ) profile of California (Boore and  
685 Joyner 1997) anchored at  $V_{s30}$  620 m/s. The base (or hard-rock) model is described in  
686 terms of seismic moments obtained from database  $M_W$ , *a priori* geometrical spreading  
687 function and regional  $Q$  models along with the station  $\kappa_0$ . To cover a broader range of  
688 stations, site-class specific site amplification factors were also estimated.

689 In the second stage of inversion, the observed Fourier spectra were corrected for site-  
690 class specific amplification factor and subsequently further inverted to obtain the  
691 Brune's corner frequency  $f_c$  and  $M_0$ . The fitting procedure involves all the records  
692 from an event where the high frequency shape of each record was constrained by using  
693 the regional  $Q$  models along with the site-class  $\kappa_0$ . Despite having very few events  
694 with a large number of multiple recordings, the inverted  $M_W$  values were found  
695 broadly consistent with the database  $M_W$ . The estimated  $\Delta\sigma$  from inverted  $f_c$  and  $M_0$   
696 did not exhibit dependence over magnitude. The database common  $\Delta\sigma$  was estimated  
697 to be 5.75 and 5.65 MPa using inverted and database  $M_W$  respectively. The  $\Delta\sigma$  values  
698 obtained in this study were observed to be in good comparison with the previous  
699 studies involving earthquakes from the same region. Although, we did not observe a  
700 clear regional dependence of  $\Delta\sigma$  mainly because of the limited dataset, the St. Die  
701 earthquake  $M_W$  4.8 located at French-German border was found to be exhibiting a  
702 relatively high  $\Delta\sigma$  of 32.3 MPa. We would like to mention here, what is already noted  
703 by Atkinson and Beresnev (1997), that the  $\Delta\sigma$  values obtained in this way do not  
704 represent the actual drop in stress (before and after the earthquake) one would expect  
705 during an earthquake rupturing, but rather a measure of the proportion of radiated high-  
706 frequencies.

707 Finally, we note that the inversion of spectral parameters in Bora et al. (2015) was  
708 focused on a record-wise fitting of each spectrum to enable a consistent extrapolation

709 beyond the filter high-pass and low frequencies. While, this study is aimed at  
710 discussing current challenges that are associated with stochastic modelling of ground  
711 motion, thus providing robust estimates of regional stochastic model parameters for  
712 Europe and Mediterranean region. Furthermore, the present study is believed to  
713 facilitate an updated reference stochastic model, presented in Table 5, for Europe and  
714 Mediterranean regions.

## 715 **10. Data and resources**

716 Data was taken from the RESORCE database (Akkar et al. 2014a). Figures were  
717 prepared using the program Mathematica except figure 1a was prepared using GMT  
718 (The Generic Mapping Tools). The linear mixed effects regression was performed  
719 using R-package *lme4* (Bates et al. 2015).

## 720 **Acknowledgements**

721 This work was funded by the SIGMA project. Dino Bindi and Olga Ktenidou are  
722 thanked for their useful discussions, comments and feedbacks.

## 723 **References**

- 724 Abrahamson NA, Silva WJ, Kamai R (2014) Summary of the ASK14 Ground Motion  
725 Relation for Active Crustal Regions. *Eq Spectra* 30:1025-1055
- 726 Aki K (1967) Scaling laws of seismic spectrum. *J Geophys Res* 72: 1217-1231
- 727 Akinci A, Malagnini L, Herrmann R, Kalafat D (2014) High-Frequency Attenuation in  
728 the Lake Van Region, Eastern Turkey. *Bull Seismol Soc Am* 104 (3):1400-1409
- 729 Akinci A., D'Amico S, Malagnini, L, Mercuri, A (2013) Scaling earthquake ground  
730 motions in western Anatolia, Turkey. *Physics and Chemistry of the Earth* 63: 124-  
731 135
- 732 Akkar S, Sandikkaya MA, Şenyurt M, Azari Sisi A, Ay BÖ, Traversa P, Douglas J,  
733 Cotton F, Luzi L, Hernandez B, Godey S (2014) Reference database for seismic  
734 ground-motion in Europe (RESORCE). *Bull Earthq Eng* 12(1): 311-339
- 735 Akkar S, Sandikkaya MA, Bommer JJ (2014b) Empirical ground-motion models for  
736 point- and extended-source crustal earthquake scenarios in Europe and the Middle  
737 East. *Bull Earthq Eng* 12 (1): 359-387
- 738 Anderson JG (1991) A preliminary descriptive model for the distance dependence of  
739 the spectral decay parameter in Southern California. *Bull Seismol Soc Am* 81:  
740 2186-2193
- 741 Anderson JG, Hough SE (1984) A model for the shape of the fourier amplitude  
742 spectrum of acceleration at high frequencies. *Bull Seismol Soc Am* 74(5): 1969-  
743 1993

744 Askan A, Sisman F, Pekcan O (2014) A regional near-surface high frequency spectral  
745 attenuation ( $\kappa$ ) model for northwestern Turkey. *Soil Dyn Earthq Eng* 65: 113-  
746 125

747 Atkinson GM (2004) Empirical Attenuation of Ground-Motion Spectral Amplitudes in  
748 Southeastern Canada and the Northeastern United States. *Bull Seismol Soc Am*  
749 94(3): 1079-1095

750 Atkinson GM, Boore DM (2011) Modifications to Existing Ground-Motion Prediction  
751 Equations in Light of New Data. *Bull Seismol Soc* 101(3) : 1121-1135

752 Atkinson GM, Morrison M (2009) Observations on Regional Variability in Ground-  
753 Motion Amplitudes for Small-to-Moderate Earthquakes in North America. *Bull*  
754 *Seismol Soc Am* 99: 2393-2409

755 Atkinson GM, Beresnev I (1997) Don't Call it Stress Drop. *Seismol Res Lett* 68(1): 3-4

756 Atkinson GM, Mereu, RF (1992) The shape of ground motion attenuation curves in  
757 Southeastern Canada. 82(5):2014-2031

758 Baltay AS, Hanks TC (2014) Understanding the magnitude dependence of PGA and  
759 PGV in NGA-West 2 data, *Bull Seismol Soc Am* 104(6): 2851-2865

760 Bates D, Maechler M, Bolker B, Walker S (2015) Fitting Linear Mixed-Effects Models  
761 Using lme4, *J Stat Softw* 67: 1-48

762 Bay F, Fäh D, Malagnini L, Giardini D (2003) Spectral Shear-Wave Ground-Motion  
763 Scaling in Switzerland. *Bull Seismol Soc* 93(1) : 414-429

764 Bindi D, Massa M, Luzi L, Ameri G, Pacor F, Puglia R, Augliera P (2014) Pan-  
765 European ground-motion prediction equations for the average horizontal component  
766 of PGA, PGV, and 5%-damped PSA at spectral periods up to 3.0 s using the  
767 RESORCE dataset. *Bull Earthq Eng* 12(1): 391-430

768 Boore DM (1983) Stochastic Simulation of high frequency ground motions based on  
769 seismological models of the radiated spectra. *Bull Seismol Soc Am* 73(6): 1865-  
770 1894

771 Boore DM (2003) Simulation of Ground Motion Using the Stochastic Method. *Pure*  
772 *Appl Geophys* 160(3): 635-676

773 Boore DM, Boatwright J (1984) Average body-wave radiation coefficients. *Bull*  
774 *Seismol Soc Am* 74(5) : 1615-1621

775 Boore DM, Joyner WB (1997) Site amplifications for generic rock sites. *Bull Seismol*  
776 *Soc Am* 87(2): 327-341

777 Boore DM, Stewart JP, Seyhan E, Atkinson GM (2014) NGA-West2 Equations for  
778 Predicting PGA, PGV, and 5% Damped PSA for Shallow Crustal Earthquakes.  
779 *Earthq Spectra* 30(3): 1057-1085

780 Bora SS, Scherbaum F, Kuehn N, Stafford P (2014) Fourier spectral- and duration  
781 models for the generation of response spectra adjustable to different source-,  
782 propagation-, and site conditions. *Bull Earthq Eng* 12(1): 467-493

783 Bora SS, Scherbaum F, Kuehn N, Stafford P, Edwards B (2015) Development of a  
784 response spectral ground-motion prediction equation (GMPE) for seismic-hazard  
785 analysis from empirical fourier spectral and duration models. *Bull Seismol Soc Am*  
786 105(4): 2192-2218

787 Brune JN (1970) Tectonic Stress and the Spectra of Seismic Shear Waves from  
788 Earthquakes. *J Geophys Res* 75(26): 4997-5009  
789 Brune JN (1971) Correction. *J Geophys Res* 76(20): 5002  
790 Campbell KW (2003) Prediction of Strong Ground Motion Using the Hybrid Empirical  
791 Method and Its Use in the Development of Ground-Motion (Attenuation) Relations  
792 in Eastern North America. *Bull Seismol Soc Am* 93(3): 1012-1033  
793 Campbell KW (2009) Estimates of shear-wave  $q$  and  $\kappa(0)$  for un- consolidated and  
794 semi-consolidated sediments in eastern North America. *Bull Seismol Soc Am* 99:  
795 2365-2392  
796 Campillo M, Bouchon M, Massinon B (1984) Theoretical study of the excitation,  
797 spectral characteristics, and geometrical attenuation of regional seismic phases. *Bull*  
798 *Seismol Soc* 74(1) : 79-90  
799 Chandler AM, Lam NT, Sang HH (2006) Near-surface attenuation modelling based on  
800 rock shear-wave velocity profile. *Soil Dyn Earthq Eng* 26: 1004-1014  
801 Chen SZ, Atkinson GM (2002) Global comparisons of earthquake source spectra. *Bull*  
802 *Seismol Soc Am* 92(3): 885-895  
803 Cotton F, Archuleta R, Causse M (2013) What is Sigma of the Stress Drop? *Seismol*  
804 *Res Lett* 84(1): 42-48  
805 Derras B, Bard PY, Cotton F (2014) Towards fully data driven ground-motion  
806 prediction models for Europe. *Bull Earthq Eng* 12(1): 495-516  
807 Douglas J, Jousset P (2011) Modeling the difference in ground-motion magnitude  
808 scaling in small and large earthquakes. *Seismol Res Lett* 82(4): 504-508  
809 Douglas J, Gehl P, Bonilla LF, Gelis C (2010) A  $\kappa$  model for mainland France.  
810 *Pure Appl Geophys* 167: 1303-1315  
811 Drouet S, Chevrot S, Cotton F, Souriau A (2008) Simultaneous inversion of source  
812 spectra, attenuation parameters, and site responses: Application to the data of the  
813 french accelerometric network. *Bull Seismol Soc Am* 98(1): 198-219  
814 Drouet S, Cotton F, Gueguen P (2010)  $\nu(S30)$ ,  $\kappa$ , regional attenuation and  $M_w$   
815 from accelerograms: application to magnitude 3-5 French earthquakes. *Geophys J*  
816 *Internat* 182(2): 880-898  
817 Edwards B, Fäh D (2013a). Measurements of stress parameter and site attenuation  
818 from recordings of moderate to large earthquakes in Europe and the Middle East.  
819 *Geophys J Internat* 194(2): 1190-1202  
820 Edwards B, Fäh D (2013b) A Stochastic Ground-Motion Model for Switzerland. *Bull*  
821 *Seismol Soc Am* 103(1): 78-98  
822 Edwards B, Rietbrock A (2009) A comparative study on attenuation and source-scaling  
823 relations in the Kanto, Tokai, and Chubu regions of Japan, using data from Hi-net  
824 and kik-net. *Bull Seismol Soc Am* 99: 2435-2460  
825 Edwards B, Rietbrock A, Bommer JJ, Baptie B (2008) The Acquisition of Source,  
826 Path, and Site Effects from Microearthquake Recordings Using Q Tomography:  
827 Application to the United Kingdom. *Bull Seismol Soc Am* 98(4): 1915-1935  
828 Edwards B, Fäh D, Giardini D (2011) Attenuation of seismic shear wave energy in  
829 Switzerland. *Geophys J Internat* 185(2): 967-984

830 Edwards B, Michel C, Poggi V, Fäh D (2013) Determination of Site Amplification  
831 from Regional Seismicity: Application to the Swiss National Seismic Networks.  
832 *Seismol Res Lett* 84(4): 611-621

833 Edwards B, Ktenidou OJ, Cotton F, Abrahamson N, Van Houtte C, Fäh D (2015)  
834 Epistemic uncertainty and limitations of the  $\kappa_0$  model for near-surface attenuation at  
835 hard rock sites. *Geophys J Internat* 202(3): 1627-1645

836 Edwards B, Cauzzi C, Danciu L, Fäh D (2016). Region-Specific Assessment,  
837 Adjustment and Weighting of Ground Motion Prediction Models: Application to the  
838 2015 Swiss Seismic Hazard Maps. *Bull Seismol Soc Am* 106(4): 1840-1857

839 Eshelby JD (1957) The determination of the elastic field of an ellipsoidal inclusion,  
840 and related problems. *Proceedings of the Royal Society of London Series*  
841 *a-Mathematical and Physical Sciences* 241: 376-396

842 a-Mathematical and Physical Sciences 241: 376-396

843 Goertz- Allmann BP, Edwards B (2014) Constraints on Crustal Attenuation and Three-  
844 Dimensional Spatial Distribution of Stress Drop in Switzerland. *Geophys J Internat*  
845 196 : 493-509

846 Hanks TC (1979)  $b$  values and  $\omega^{-y}$  seismic source models: Implications for tectonic  
847 stress variations along active crustal fault zones and the estimation of high-  
848 frequency strong ground motion. *J Geophys Res* 84: 2235-2242

849 Hanks TC, Kanamori H (1979) A moment magnitude scale. *J Geophys Res B: Solid*  
850 *Earth* 84: 2348-2350

851 Hanks TC, McGuire RK (1981) The character of high-frequency strong ground  
852 motion. *Bull Seismol Soc Am* 71(6): 2071-2095

853 Hatzidimitrou, PM (1995) S-Wave Attenuation in the crust in northern Greece. *Bull*  
854 *Seismol Soc Am* 85(5) : 1381-1387

855 Hermkes M, Kuehn N, Riggelsen C (2014) Simultaneous quantification of epistemic  
856 and aleatory uncertainty in GMPEs using Gaussian process regression. *Bull Earthq*  
857 *Eng* 12: 449-466

858 Hough SE, Anderson JG, Brune J, Vernon F, Berger J, Fletcher J, Haar L, Hanks L,  
859 Baker L (1988) Attenuation near Anza, California. *Bull Seismol Soc Am* 78(2):  
860 672-691

861 Joyner WB, Warrick RE, Fumal TE (1981) The effect of quaternary alluvium on  
862 strong ground motion in the Coyote Lake, California, earthquake of 1979. *Bull*  
863 *Seismol Soc Am* 71(4): 1333-1349

864 Kilb D, Glenn B, Anderson JG, Brune J, Zhigang P, Vernon F (2012) A comparison of  
865 spectral parameter  $\kappa$  from small and moderate earthquakes using Southern  
866 California ANZA seismic network data. *Bull Seismol Soc Am* 102(1): 284-300

867 Konno K, Ohmachi T (1998) Ground-motion characteristics estimated from spectral  
868 ratio between horizontal and vertical components of microtremor. *Bull Seismol Soc*  
869 *America* 88(1): 228-241

870 Kotha SR, Bindi D, Cotton F (2016) Partially non-ergodic region specific GMPE for  
871 Europe and Middle-East. *Bull Earthq Eng* 14(4): 1245-1263

872 Ktenidou O-J, Abrahamson NA, Drouet S, Cotton F (2015) Understanding the physics  
873 of  $\kappa$  ( $\kappa$ ): insights from a downhole array. *Geophys J Internat* 203 : 678-691.



874 Ktenidou O-J, Cotton F, Abrahamson NA, Anderson JG (2014) Taxonomy of kappa: A  
875 Review of Definitions and Estimation Approaches Targeted to Applications.  
876 *Seismol Res Lett* 85(1): 135-146

877 Kurtulmus, TÖ and Akyol, N. Crustal attenuation characteristics in western Turkey.  
878 *Geophys J Internat* 195 : 1384-1395

879 Kuehn N, Scherbaum F (2016) A partially non-ergodic ground-motion prediction  
880 equation for Europe and the Middle East. *Bull Earthq Eng* 14(10): 2629-2641

881 Malagnini L, Herrmann RB (2000) Ground-Motion Scaling in the Region of the 1997  
882 Umbria-Marche Earthquake (Italy). *Bull Seismol Soc America* 90(4): 1041-1051

883 Malagnini L, Herrmann RB, Koch K (2000) Regional Ground-Motion Scaling in  
884 Central Europe. *Bull Seismol Soc America* 90(4) : 1052-1061

885 Malagnini L, Akinci A, Herrmann RB, Pino NA, Scognamiglio L (2002)  
886 Characteristics of the Ground Motion in Northeastern Italy. *Bull Seismol Soc*  
887 *America* 92(6) : 2186-2204

888 Malagnini L, Scognamiglio L, Mercuri A, Akinci A, Mayeda K (2008) Strong  
889 evidence for non-similar earthquake source scaling in central Italy. *Geophys Res*  
890 *Lett* 35: L17303

891 Malagnini L, Akinci A, Mayeda K, Munafo I, Herrmann RB and Mercuri A (2011)  
892 Characterization of earthquake-induced ground motion from the L'Aquila seismic  
893 sequence of 2009, Italy. *Geophys J Internat* 184 : 325-337

894 Margaris BN, Boore D (1998) Determination of  $\Delta\sigma$  and  $\kappa_0$  from response spectra of  
895 large earthquakes in Greece. *Bull Seismol Soc Am* 88(1) : 170-182

896 McGuire RK, & Hanks TC (1980). RMS acceleration and spectral amplitudes of strong  
897 ground-motion during the San Fernando, California earthquake. *Bull Seismol Soc*  
898 *Am* 70(5): 1907-1919

899 Molkenhain C, Scherbaum F, Griewank A, Kuehn N, Stafford P J. (2014) A Study of  
900 the Sensitivity of Response Spectral Amplitudes on Seismological Parameters  
901 Using Algorithmic Differentiation. *Bull Seismol Soc Am* 104(5): 2240-2252

902 Morozov IB (2008) Geometrical attenuation, frequency dependence of Q, and the  
903 absorption band problem. *Geophys J Internat* 175 : 239-252

904 Morozov IB (2009) Thirty years of confusion around “scattering Q”? *Seism Res Lett*  
905 80 : 5-7

906 Pacor F, Spallarossa D, Oth A, Luzi L, Puglia R, Cantore L, Mercuri A, D'Amico M,  
907 Bindi D (2016) Spectral models for ground motion prediction in the L'Aquila  
908 region (central Italy): evidence for stress-drop dependence on magnitude and depth.  
909 *Geophys J Internat* 204 : 697-718

910 Parolai S, Bindi D (2004) Influence of Soil-Layer Properties on k Evaluation. *Bull*  
911 *Seismol Soc America* 94(1): 349-356

912 Poggi V, Edwards B, Fäh D (2011) Derivation of a Reference Shear-Wave Velocity  
913 Model from Empirical Site Amplification. *Bull Seismol Soc Am* 101(1): 258-274

914 Polatidis A, Kiratzi A, Hatzidimitriou PM, Margaris B (2003) Attenuation of shear-  
915 waves in the back-arc region of the Hellenic arc for frequencies from 0.6 to 16 Hz.  
916 *Tectonophysics* 367 : 29-40

917 Scherbaum F, Schmedes J, Cotton F (2004) On the conversion of source-to-site  
918 distance measures for extended earthquake source models. Bull Seismol Soc  
919 America 94(3): 1053-1069  
920 Singh SK, Apsel J, Fried J, Brune, JN (1982) Spectral attenuation of SH waves along  
921 the Imperial fault. Bull Seismol Soc America 72(6): 2003-2016  
922 Van Houtte C, Drouet S, Cotton F (2011) Analysis of the Origins of kappa (Kappa) to  
923 Compute Hard Rock to Rock Adjustment Factors for GMPEs. Bull Seismol Soc  
924 America 101(6): 2926-2941  
925 Yenier E, Atkinson GM (2015a) An Equivalent Point-Source Modeling of Moderate-  
926 to-Large Magnitude Earthquakes and Associated Ground-Motion Saturation  
927 Effects. Bull Seismol Soc Am 105(3): 1435-1455  
928 Yenier E, Atkinson GM (2015b) Regionally adjustable generic ground-motion  
929 prediction equation based on equivalent point-source simulations: application to  
930 central and eastern North America. Bull Seismol Soc Am 105(4): 1989-2009.  
931  
932

**Table 1** Station specific  $\kappa_0$  estimation for stations recording at least seven records.

| Station Id | Station Country | $V_{S30}$ (m/s) | N  | $\kappa_0$ (s) |               |               |
|------------|-----------------|-----------------|----|----------------|---------------|---------------|
|            |                 |                 |    | 50 Percentile  | 16 Percentile | 84 Percentile |
| 3          | Italy           | 1029.6          | 14 | 0.022          | 0.016         | 0.032         |
| 19         | Italy           | 162.1           | 14 | 0.027          | 0.018         | 0.039         |
| 129        | Italy           | 444.7           | 14 | 0.027          | 0.018         | 0.03          |
| 148        | Turkey          | 283.3           | 14 | 0.03           | 0.022         | 0.039         |
| 184        | Turkey          | 316             | 14 | 0.029          | 0.026         | 0.038         |
| 187        | Turkey          | 481.3           | 14 | 0.021          | 0.017         | 0.025         |
| 190        | Turkey          | 616.4           | 14 | 0.037          | 0.031         | 0.049         |
| 3633       | Italy           | 679.2           | 14 | 0.031          | 0.019         | 0.037         |
| 10         | Italy           | 600             | 16 | 0.029          | 0.028         | 0.037         |
| 146        | Turkey          | 282             | 16 | 0.027          | 0.022         | 0.08          |
| 162        | Turkey          | 338.6           | 16 | 0.02           | 0.008         | 0.032         |
| 188        | Turkey          | 293.6           | 16 | 0.063          | 0.02          | 0.081         |
| 2462       | Turkey          | 354.8           | 16 | 0.04           | 0.034         | 0.059         |
| 2635       | Turkey          | 228.7           | 16 | 0.032          | 0.03          | 0.049         |
| 3612       | Italy           | 835.5           | 16 | 0.022          | 0.02          | 0.03          |
| 124        | Italy           | 219.3           | 18 | 0.029          | 0.023         | 0.037         |
| 136        | Turkey          | 285.5           | 18 | 0.045          | 0.032         | 0.111         |
| 147        | Turkey          | 408.7           | 18 | 0.039          | 0.033         | 0.049         |
| 169        | Turkey          | 338.6           | 18 | 0.03           | 0.019         | 0.037         |
| 105        | Turkey          | 355.9           | 20 | 0.038          | 0.03          | 0.068         |
| 3620       | Italy           | 199             | 20 | 0.044          | 0.006         | 0.055         |
| 183        | Turkey          | 455.7           | 21 | 0.032          | 0.026         | 0.043         |
| 120        | Italy           | 142.6           | 22 | 0.03           | 0.019         | 0.043         |
| 231        | Turkey          | 407.3           | 22 | 0.046          | 0.035         | 0.072         |
| 2503       | Turkey          | 480.8           | 22 | 0.041          | 0.032         | 0.048         |
| 2987       | Italy           | 684.8           | 22 | 0.013          | 0.008         | 0.032         |
| 3679       | Italy           | 488             | 22 | 0.01           | 0.004         | 0.026         |
| 2465       | Turkey          | 267.4           | 24 | 0.041          | 0.036         | 0.051         |
| 3614       | Italy           | 473.7           | 24 | 0.014          | 0.009         | 0.036         |
| 138        | Turkey          | 242.5           | 26 | 0.066          | 0.047         | 0.083         |
| 140        | Turkey          | 456.6           | 26 | 0.051          | 0.043         | 0.059         |
| 2322       | Turkey          | 746.9           | 26 | 0.05           | 0.04          | 0.071         |
| 2459       | Turkey          | 366.9           | 27 | 0.038          | 0.033         | 0.044         |
| 229        | Turkey          | 528.7           | 28 | 0.042          | 0.033         | 0.052         |
| 2591       | Turkey          | 374.9           | 28 | 0.062          | 0.054         | 0.065         |
| 2466       | Turkey          | 232.9           | 30 | 0.04           | 0.022         | 0.053         |
| 2984       | Italy           | 716.5           | 30 | 0.019          | 0.009         | 0.033         |
| 122        | Italy           | 554.8           | 32 | 0.021          | 0.014         | 0.026         |
| 149        | Turkey          | 595.2           | 34 | 0.03           | 0.024         | 0.048         |
| 153        | Turkey          | 191.8           | 34 | 0.046          | 0.034         | 0.067         |
| 8          | Italy           | 454.4           | 40 | 0.021          | 0.018         | 0.031         |
| 139        | Turkey          | 662             | 40 | 0.048          | 0.04          | 0.064         |
| 155        | Turkey          | 412             | 40 | 0.03           | 0.023         | 0.041         |
| 131        | Italy           | 534             | 42 | 0.012          | 0.008         | 0.02          |

| Station Id | Station<br>Country | $V_{S30}$<br>(m/s) | $N$ | $\kappa_0$ (s)   |                  |                  |
|------------|--------------------|--------------------|-----|------------------|------------------|------------------|
|            |                    |                    |     | 50<br>Percentile | 16<br>Percentile | 84<br>Percentile |
| 134        | Turkey             | 270                | 56  | 0.059            | 0.045            | 0.074            |

934  
935

936 **Table 2** Site-class specific estimates of  $\kappa_0$  in each regional subset.

| Site Class     | $\kappa_0$ (s) |        |        |        |       |        |        |        |           |        |        |        |
|----------------|----------------|--------|--------|--------|-------|--------|--------|--------|-----------|--------|--------|--------|
|                | Turkey         |        |        |        | Italy |        |        |        | Remaining |        |        |        |
|                | N              | 16 Per | 50 Per | 84 Per | N     | 16 Per | 50 Per | 84 Per | N         | 16 Per | 50 Per | 84 Per |
| Very soft soil | 14             | 0.0273 | 0.0395 | 0.0472 | 32    | 0.0185 | 0.029  | 0.0618 | 0         | -      | -      | -      |
| Soft soil      | 330            | 0.0265 | 0.0433 | 0.0675 | 83    | 0.0172 | 0.0271 | 0.0436 | 43        | 0.011  | 0.0267 | 0.0469 |
| Stiff Soil     | 315            | 0.0275 | 0.0416 | 0.0605 | 219   | 0.0099 | 0.0224 | 0.0387 | 96        | 0.0122 | 0.0271 | 0.0429 |
| Rock           | 8              | 0.0317 | 0.0495 | 0.0662 | 38    | 0.0076 | 0.0212 | 0.0322 | 22        | 0.0048 | 0.0232 | 0.0447 |

**Table 3** Stress parameter values for earthquakes recorded on at least seven stations. Min and Max correspond to the 68% confidence limit in fitted  $M_W$  and  $f_c$ .

| Eq. Id | Eq. Country | Eq. Name    | Y    | M   | D  | H  | M  | S  | Depth $h$ (km) | N  | Inverted $M_W$ |            |            |       | Database $M_W$ |                      |                      |     |       |                |                      |                      |
|--------|-------------|-------------|------|-----|----|----|----|----|----------------|----|----------------|------------|------------|-------|----------------|----------------------|----------------------|-----|-------|----------------|----------------------|----------------------|
|        |             |             |      |     |    |    |    |    |                |    | $M_W$          | $M_{WMin}$ | $M_{WMax}$ | $f_c$ | $\Delta\sigma$ | $\Delta\sigma_{Min}$ | $\Delta\sigma_{Max}$ | M   | $f_c$ | $\Delta\sigma$ | $\Delta\sigma_{Min}$ | $\Delta\sigma_{Max}$ |
| 57     | Italy       | Friuli      | 1976 | 09  | 15 | 09 | 21 | 18 | 7              | 16 | 5.77           | 5.74       | 5.8        | 0.51  | 13.38          | 11.5                 | 15.57                | 6   | 0.34  | 8.6            | 8.41                 | 8.8                  |
| 96     | Italy       | NA          | 1981 | 01  | 16 | 00 | 37 | 45 | 10.5           | 14 | 5.33           | 5.3        | 5.36       | 0.56  | 3.9            | 3.3                  | 4.6                  | 5.2 | 0.71  | 5.06           | 4.93                 | 5.2                  |
| 531    | Italy       | Umbria      | 1997 | 09  | 26 | 00 | 33 | 12 | 7              | 18 | 5.94           | 5.91       | 5.98       | 0.26  | 3.37           | 2.83                 | 4.02                 | 5.7 | 0.41  | 5.27           | 5.18                 | 5.36                 |
| 533    | Italy       | Umbria      | 1997 | 09  | 26 | 09 | 40 | 25 | 6              | 18 | 6.05           | 6.02       | 6.08       | 0.24  | 3.52           | 2.93                 | 4.21                 | 6   | 0.26  | 3.85           | 3.79                 | 3.91                 |
| 543    | Italy       | App.        | 1997 | 10  | 06 | 23 | 24 | 53 | 3.9            | 16 | 5.75           | 5.71       | 5.78       | 0.31  | 2.77           | 2.29                 | 3.35                 | 5.4 | 0.57  | 5.3            | 5.2                  | 5.4                  |
| 551    | Italy       | Umbria      | 1997 | 10  | 14 | 15 | 23 | 09 | 7.3            | 14 | 6.11           | 6.07       | 6.15       | 0.18  | 1.92           | 1.57                 | 2.33                 | 5.6 | 0.44  | 4.78           | 4.72                 | 4.84                 |
| 927    | Turkey      | Kocaeli     | 1999 | 08  | 17 | 00 | 01 | 39 | 17             | 33 | 7.53           | 7.5        | 7.56       | 0.06  | 9.12           | 7.77                 | 10.71                | 7.6 | 0.05  | 8.11           | 8.06                 | 8.16                 |
| 970    | Turkey      | Izmit       | 1999 | 08  | 19 | 15 | 17 | 45 | 12             | 16 | 5.36           | 5.35       | 5.38       | 0.36  | 1.17           | 1.08                 | 1.28                 | 5.1 | 0.58  | 1.95           | 1.93                 | 1.97                 |
| 982    | Turkey      | Izmit       | 1999 | 08  | 22 | 14 | 31 | 00 | 14             | 14 | 5.27           | 5.25       | 5.29       | 0.47  | 1.81           | 1.64                 | 2.01                 | 4.1 | 4.32  | 25.2           | 24.32                | 26.28                |
| 1056   | Turkey      | Izmit       | 1999 | 08  | 31 | 08 | 10 | 49 | 4              | 30 | 5.25           | 5.24       | 5.26       | 0.63  | 4.24           | 4                    | 4.5                  | 5.1 | 0.84  | 5.81           | 5.75                 | 5.87                 |
| 1115   | Greece      | Ano         | 1999 | 09  | 07 | 11 | 56 | 51 | 17             | 18 | 5.77           | 5.75       | 5.78       | 0.59  | 20.19          | 18.35                | 22.21                | 6   | 0.39  | 12.7           | 12.58                | 12.99                |
| 1146   | Turkey      | Izmit       | 1999 | -09 | 13 | 11 | 55 | 30 | 14             | 54 | 6.12           | 6.11       | 6.14       | 0.26  | 6.19           | 5.7                  | 6.72                 | 5.8 | 0.47  | 11.2           | 11.14                | 11.31                |
| 1172   | Turkey      | Izmit       | 1999 | 09  | 20 | 21 | 28 | 00 | 15             | 24 | 5.43           | 5.41       | 5.44       | 0.43  | 2.44           | 2.21                 | 2.69                 | 4.8 | 1.32  | 8.1            | 7.98                 | 8.22                 |
| 1203   | Turkey      | Izmit       | 1999 | 09  | 29 | 00 | 13 | 06 | 12             | 14 | 5.7            | 5.67       | 5.73       | 0.35  | 3.32           | 2.84                 | 3.88                 | 5.2 | 0.85  | 8.47           | 8.32                 | 8.62                 |
| 1245   | Turkey      | Izmit       | 1999 | 11  | 07 | 16 | 54 | 41 | 7              | 22 | 4.59           | 4.58       | 4.6        | 2.02  | 14.13          | 13.32                | 14.97                | 4.9 | 1.08  | 6.3            | 6.19                 | 6.42                 |
| 1256   | Turkey      | Izmit       | 1999 | 11  | 11 | 14 | 41 | 23 | 8              | 46 | 5.85           | 5.84       | 5.86       | 0.35  | 5.76           | 5.36                 | 6.2                  | 5.6 | 0.55  | 9.23           | 9.15                 | 9.3                  |
| 1427   | Turkey      | Duzce       | 1999 | 11  | 13 | 00 | 54 | 54 | 5              | 14 | 4.6            | 4.58       | 4.61       | 2.37  | 23.14          | 21.24                | 25.17                | 5   | 1.04  | 7.97           | 7.75                 | 8.21                 |
| 1484   | Turkey      | Duzce       | 1999 | 11  | 16 | 17 | 51 | 17 | 5              | 16 | 5.01           | 4.99       | 5.03       | 0.74  | 2.9            | 2.62                 | 3.22                 | 5   | 0.75  | 2.95           | 2.9                  | 3.01                 |
| 1501   | Turkey      | Duzce       | 1999 | 11  | 19 | 19 | 59 | 06 | 5              | 20 | 4.72           | 4.71       | 4.73       | 1.6   | 10.76          | 9.97                 | 11.61                | 4.9 | 1.11  | 6.83           | 6.68                 | 6.98                 |
| 2065   | Turkey      | Duzce       | 2000 | 08  | 23 | 13 | 41 | 28 | 15             | 14 | 5.97           | 5.93       | 6.01       | 0.19  | 1.4            | 1.15                 | 1.71                 | 5.5 | 0.44  | 3.27           | 3.23                 | 3.32                 |
| 2454   | Turkey      | Demirtas    | 2001 | 06  | 22 | 11 | 54 | 50 | 10             | 16 | 5.44           | 5.42       | 5.45       | 0.34  | 1.27           | 1.17                 | 1.38                 | 5.2 | 0.52  | 1.99           | 1.97                 | 2.01                 |
| 2814   | Turkey      | Seferihisar | 2003 | 04  | 10 | 00 | 40 | 14 | 10             | 14 | 5.84           | 5.82       | 5.86       | 0.34  | 4.8            | 4.38                 | 5.26                 | 5.7 | 0.43  | 6.21           | 6.14                 | 6.28                 |
| 2959   | Turkey      | NA          | 2003 | 06  | 09 | 17 | 44 | 03 | 9.1            | 16 | 4.82           | 4.82       | 4.83       | 1.49  | 12.58          | 11.98                | 13.22                | 4.8 | 1.56  | 13.3           | 13.17                | 13.57                |
| 3004   | Turkey      | NA          | 2003 | 07  | 23 | 04 | 56 | 05 | 28.3           | 14 | 5.31           | 5.29       | 5.32       | 0.95  | 17.55          | 16.33                | 18.85                | 5.3 | 0.96  | 17.7           | 17.47                | 18.1                 |
| 3037   | Turkey      | NA          | 2003 | 07  | 26 | 01 | 00 | 57 | 5              | 14 | 4.84           | 4.83       | 4.85       | 1.32  | 9.24           | 8.65                 | 9.87                 | 4.9 | 1.17  | 8.01           | 7.86                 | 8.16                 |

| Eq. Id | Eq. Country | Eq. Name   | Y    | M  | D  | H  | M  | S  | Depth $h$ (km) | N  | Inverted $M_W$ |            |           |       |                |                      | Database $M_W$      |     |       |                |                      |                     |
|--------|-------------|------------|------|----|----|----|----|----|----------------|----|----------------|------------|-----------|-------|----------------|----------------------|---------------------|-----|-------|----------------|----------------------|---------------------|
|        |             |            |      |    |    |    |    |    |                |    | $M_W$          | $M_{WMIn}$ | $M_{WMa}$ | $f_c$ | $\Delta\sigma$ | $\Delta\sigma_{Min}$ | $\Delta\sigma_{Ma}$ | M   | $f_c$ | $\Delta\sigma$ | $\Delta\sigma_{Min}$ | $\Delta\sigma_{Ma}$ |
| 3054   | Turkey      | NA         | 2003 | 07 | 26 | 08 | 36 | 10 | 21.3           | 14 | 5.46           | 5.45       | 5.47      | 0.8   | 17.69          | 16.52                | 18.93               | 5.4 | 0.9   | 20.1           | 19.82                | 20.45               |
| 3405   | Turkey      | NA         | 2004 | 12 | 20 | 23 | 02 | 15 | 12.5           | 16 | 5.56           | 5.54       | 5.57      | 0.46  | 4.74           | 4.36                 | 5.15                | 5.3 | 0.73  | 7.84           | 7.74                 | 7.95                |
| 3553   | Turkey      | NA         | 2006 | 02 | 08 | 04 | 07 | 42 | 6.8            | 14 | 4.35           | 4.35       | 4.36      | 2.83  | 17.24          | 16.33                | 18.18               | 4.5 | 2.06  | 10.9           | 10.75                | 11.17               |
| 3641   | Turkey      | NA         | 2006 | 10 | 20 | 18 | 15 | 26 | 16.7           | 36 | 5.03           | 5.03       | 5.04      | 0.91  | 6.03           | 5.83                 | 6.24                | 4.9 | 1.17  | 8.02           | 7.96                 | 8.09                |
| 3650   | Turkey      | NA         | 2006 | 10 | 24 | 14 | 00 | 22 | 7.9            | 52 | 4.9            | 4.9        | 4.9       | 1.51  | 17.02          | 16.64                | 17.41               | 5.2 | 0.84  | 8.44           | 8.38                 | 8.49                |
| 3774   | Turkey      | NA         | 2007 | 11 | 09 | 01 | 43 | 05 | 15.9           | 16 | 5.01           | 5          | 5.01      | 1.02  | 7.7            | 7.37                 | 8.04                | 5.2 | 0.71  | 5.06           | 5.01                 | 5.12                |
| 3932   | Montenegro  | Montenegro | 1979 | 05 | 24 | 17 | 23 | 18 | 5              | 14 | 5.74           | 5.73       | 5.76      | 0.63  | 22.88          | 20.74                | 25.22               | 6.2 | 0.28  | 9.39           | 9.21                 | 9.58                |
| 4699   | Italy       | L          | 2009 | 04 | 06 | 01 | 32 | 39 | 8.8            | 14 | 6.33           | 6.3        | 6.37      | 0.14  | 2.11           | 1.8                  | 2.49                | 6.3 | 0.15  | 2.25           | 2.22                 | 2.27                |
| 4703   | Italy       | L          | 2009 | 04 | 07 | 09 | 26 | 28 | 10.2           | 14 | 5.01           | 5          | 5.02      | 0.62  | 1.75           | 1.64                 | 1.87                | 5   | 0.63  | 1.79           | 1.77                 | 1.82                |
| 4704   | Italy       | L          | 2009 | 04 | 07 | 17 | 47 | 37 | 15.1           | 28 | 5.5            | 5.49       | 5.51      | 0.49  | 4.76           | 4.52                 | 5.02                | 5.6 | 0.41  | 3.96           | 3.93                 | 4                   |
| 4705   | Italy       | Aquila     | 2009 | 04 | 07 | 21 | 34 | 29 | 7.4            | 16 | 4.59           | 4.58       | 4.6       | 1.22  | 3.07           | 2.9                  | 3.24                | 4.6 | 1.19  | 2.98           | 2.94                 | 3.03                |
| 4706   | Italy       | Aquila     | 2009 | 04 | 08 | 22 | 56 | 50 | 10.2           | 14 | 4.16           | 4.15       | 4.17      | 2.08  | 3.48           | 3.32                 | 3.66                | 4.1 | 2.36  | 4.12           | 4.04                 | 4.19                |
| 4707   | Italy       | Gran       | 2009 | 04 | 09 | 00 | 52 | 59 | 15.4           | 26 | 5.54           | 5.53       | 5.56      | 0.37  | 2.35           | 2.19                 | 2.52                | 5.4 | 0.48  | 3.06           | 3.03                 | 3.09                |
| 4709   | Italy       | Aquila     | 2009 | 04 | 09 | 04 | 32 | 44 | 8.1            | 14 | 4.43           | 4.42       | 4.44      | 1.22  | 1.79           | 1.69                 | 1.89                | 4.2 | 1.91  | 3.08           | 3.03                 | 3.14                |
| 4710   | Italy       | Aquila     | 2009 | 04 | 09 | 19 | 38 | 16 | 17.2           | 18 | 5.07           | 5.06       | 5.08      | 0.74  | 3.55           | 3.37                 | 3.75                | 5.3 | 0.48  | 2.21           | 2.19                 | 2.24                |
| 4747   | Turkey      | Kovancilar | 2010 | 03 | 08 | 02 | 32 | 39 | 5              | 14 | 6.3            | 6.27       | 6.32      | 0.15  | 2.11           | 1.84                 | 2.42                | 6.1 | 0.21  | 3.01           | 2.98                 | 3.04                |
| 4749   | Turkey      | Simav      | 2011 | 05 | 19 | 20 | 15 | 23 | 12             | 86 | 5.82           | 5.81       | 5.83      | 0.4   | 7.61           | 7.35                 | 7.88                | 5.9 | 0.35  | 6.52           | 6.49                 | 6.56                |
| 4993   | France      | St. Die    | 2003 | 02 | 22 | 20 | 41 |    | 5              | 18 | 4.955          | 4.94       | 4.96      | 1.75  | 32.3           | 30.88                | 33.78               | 4.8 | 2.41  | 49.2           | 48.42                | 49.98               |

938 **Table 4:** Seismological parameters derived from different studies.

|                               | Region                   | $G(R)$   | $Q$  | $\kappa_0$ (s) | $\Delta\sigma$ (MPa) |
|-------------------------------|--------------------------|--|--|----------------|----------------------|
| Kurtulmus and Akyol (2013)    | Western Turkey           | Frequency dependent ranging from 0.84 to 1.52 at $R \leq 200$ km   | $60f^{1.4}$  |                |                      |
| Akinci et al. (2014)          | Eastern Turkey           | $G(R) = \begin{cases} R^{-1} & R < 40 \text{ km} \\ R^{-0.3} & 40 < R < 200 \text{ km} \end{cases}$  | $Q(10) = 1507$<br>$100f^{0.43}$<br>$Q(10) = 269$                                   | 0.03           | 4-20                 |
| Akinci et al. (2013)          | Anatolia, Turkey         | $G(R) = \begin{cases} R^{-1} & R \leq 20 \text{ km} \\ R^{-0.8} & 20 \leq R \leq 40 \text{ km} \\ R^{-0.7} & 40 \leq R \leq 100 \text{ km} \\ R^{-0.5} & R \geq 100 \text{ km} \end{cases}$  | $180f^{0.55}$<br>$Q(10) = 639$   | 0.045          | 10                   |
| Askan et al. (2014)           | Northwestern Turkey      |  | 2164<br>soft soil  | 0.0455         |                      |
| Hatzidimitriou (1995)         | Northern Greece          | $G(R) = R^{-1}$ $10 \leq R \leq 70$ km   | $85f^{0.91}$   |                |                      |
| Margaris and Boore (1998)     | Greece                   | $G(R) = R^{-1}$ $R \leq 50$ km   | $Q(10) = 691$<br>$88f^{0.9}$   | 0.06           | 5.6                  |
| Polatidis et al. (2003)       | Hellenic arc Greece      | $G(R) = \begin{cases} R^{-1} & R \leq 100 \text{ km} \\ R^{-2} & R > 100 \text{ km} \end{cases}$   | $Q(10) = 700$<br>$55f^{0.91}$<br>$Q(10) = 447$                                     |                |                      |
| Malagnini et al. (2000)       | Central Europe           | $G(R) = \begin{cases} R^{-0.8} & R \leq 140 \text{ km} \\ R^{-1.5} & 140 \leq R \leq 180 \text{ km} \\ R^0 & 180 \leq R \leq 220 \text{ km} \\ R^{-0.5} & R \geq 220 \text{ km} \end{cases}$ | $400f^{0.42}$<br>$Q(10) = 1052$  | 0.05           | 3                    |
| Edwards and Fäh (2013a)       | Europe and Middle East   | $R^{-1}$ $R < 100$ km  | 619-716  | 0.032-0.033    | 8.8                  |
| Malagnini and Herrmann (2000) | Umbria-Marche Italy      | $R^{-1}$ $R < 50$ km   | $130f^{0.1}$   | 0.04           | 20                   |
| Malagnini et al. (2002)       | Northeastern Italy       | Frequency and distance dependent at $R \leq 200$ km  | $Q(10) = 164$<br>$260f^{0.55}$   | 0.045          | 60                   |
| Malagnini et al. (2011)       | L'Aquila                 | $G(R) = \begin{cases} R^{-1.1} & R \leq 10 \text{ km} \\ R^{-1} & 10 \leq R \leq 30 \text{ km} \\ R^{-0.7} & R > 30 \text{ km} \end{cases}$  | $Q(10) = 922$<br>$140f^{0.25}$<br>$Q(10) = 249$                                    |                |                      |
| Pacor et al. (2016)           | L'Aquila                 | $G(R) = \begin{cases} R^{-1.08} & R \leq 10 \text{ km} \\ R^{-1.64} & 10 \leq R \leq 70 \text{ km} \\ R^{-0.64} & R > 70 \text{ km} \end{cases}$   | $290f^{0.16}$<br>$Q(10) = 419$   | 0.012          | 0.1-25               |
| This study                    | Europe and Mediterranean | $G(R) = \begin{cases} R^{-1.14} & R \leq 70 \text{ km} \\ R^{-0.5} & 70 < R \leq 225 \text{ km} \end{cases}$   | $\begin{cases} 610 & R \leq 40 \text{ km} \\ 1152 & R > 40 \text{ km} \end{cases}$ | 0.031          | 5.65                 |
| This study                    | Italy                    | $G(R) = \begin{cases} R^{-1.14} & R \leq 70 \text{ km} \\ R^{-0.5} & 70 < R \leq 225 \text{ km} \end{cases}$   | 601  | 0.026          |                      |
| This study                    | Turkey                   | $G(R) = \begin{cases} R^{-1.14} & R \leq 70 \text{ km} \\ R^{-0.5} & 70 < R \leq 225 \text{ km} \end{cases}$   | 1462   | 0.046          |                      |



|     |            |                                 |   |     |       |
|-----|------------|---------------------------------|---|-----|-------|
| 939 | This study | Remaining<br>(mainly<br>Greece) | $G(R)$<br>= $\begin{cases} R^{-1.14} & R \leq 70 \text{ km} \\ R^{-0.5} & 70 < R \leq 225 \text{ km} \end{cases}$ | 780 | 0.033 |
|-----|------------|---------------------------------|---|-----|-------|

940 **Table 5** Seismological parameters for Europe and Mediterranean stochastic model.

| Parameter                         | Parameter Estimate   |
|-----------------------------------|--|
| Source spectrum                   | Brune single corner $f_c$ point source   |
| Stress parameter $\Delta\sigma$   | 5.75 MPa with inverted $M_W$ , Std. Dev. 0.43 in log units<br>5.65 MPa with database $M_W$ , Std. Dev. 0.33 in log units                                       |
| Geometrical spreading             | $R^{-1.14}$ for $R \leq 70$ km<br>$R^{-0.5}$ for $R > 70$ km   |
| Inelastic attenuation $Q_0$       | 610 for $R \leq 40$ km<br>1152 for $R > 40$ km<br>For Turkey:<br>1462; 68% confidence limits: 1333, 1620<br>For Italy:<br>601; 68% confidence limits: 566, 640 |
| Shear wave velocity $\beta$       | 3.5 km/s   |
| Density $\rho$                    | 2800 kg/m <sup>3</sup>   |
| Site attenuation $\kappa_0$ (s)   | 0.0308, Standard Error: 0.0024<br>For Turkey:<br>0.0457, Standard Error: 0.002<br>For Italy:<br>0.0261, Standard Error: 0.0015                                 |
| Site amplification                | Station and site-class specific from residual analysis   |
| Reference rock site amplification | California generic rock anchored at $V_{S30}$ 620 m/s (Boore and Joyner 1997)  |

941